AIMS Mathematics, 10(5): 12493–12518.
DOI:10.3934/math.2025564
Received: 21 March 2025
Revised: 03 May 2025
Accepted: 09 May 2025
Published: 28 May 2025

https://www.aimspress.com/journal/Math

Research article

Multiplicity of kink and hump structures in Van der Waals gas system

Rashid Ali[1], Rabia Imtiaz[2], Moin-ud-Din Junjua[1,3,*], Fuad A. Awwad[4], Emad A. A. Ismail[4] and Ahmed S. Hendy[5,6]

[1] School of Mathematical Sciences, Zhejiang Normal University, Jinhua 321004, Zhejiang, China
[2] Department of Mathematics, University of Engineering and Technology, Lahore 39161, Pakistan
[3] Department of Mathematics, Ghazi University, Dera Ghazi Khan 32200, Pakistan
[4] Department of Quantitative Analysis, College of Business Administration, King Saud University, P.O. Box 71115, Riyadh 11587, Saudi Arabia
[5] Department of Computational Mathematics and Computer Science, Institute of Natural Sciences and Mathematics, Ural Federal University, 19 Mira St., Yekaterinburg 620002, Russia
[6] Department of Mechanics and Mathematics, Western Caspian University, Baku 1001, Azerbaijan

* **Correspondence:** Email: moinuddin@zjnu.edu.cn.

Abstract: In this work, numerous features of the nonlinear Van der Waals gas system in the sense of viscosity capillarity are analytically and theoretically investigated. A novel trustworthy integrating approach, namely the Riccati modified extended simple equation method (RMESEM), is utilized to determine the physical nature of the system. This technique successfully generates a novel range of kink, anti-kink, cuspon kink, and bell-shaped bright and dark hump solitary wave solutions in the form of exponential, periodic, hyperbolic, rational, and rational-hyperbolic functions. Using suitable parameter values that satisfy constraint criteria, we generate a set of 2D graphs to improve comprehension and graphically depict these solitary wave solutions. The efficiency and adaptability of our method in solving a range of nonlinear problems in mathematical science and engineering are validated by our computational research.

Keywords: Van der Waals gas system; nonlinear partial differential equation; Riccati modified extended simple equation method; kink and hump solitons; Riccati equation
Mathematics Subject Classification: 34G20, 35A20, 35A22, 35R11

1. Introduction

Nonlinear partial differential equations (NPDEs) are used to simulate complex processes that represent a variety of physical phenomena in a broad range of scientific domains. NPDEs are widely

applied in several fields, including optics [1], finance [2], engineering science [3], and machine learning [4]. Determining exact solutions to NPDEs is a crucial area of research as analytical solutions disclose the physical properties of nonlinear systems [5]. A number of effective techniques have been employed to ascertain the analytical results for NPDEs, including the unified Riccati equation expansion method [6], the extended direct algebraic method (EDAM) [7–9], the Painlevé approach [10], RMESEM [11], the (G'/G) expansion method [12–14], the Lie symmetry approach [15], and numerous other methods [16–18].

In physics and mathematics, a solitary wave is a non-dispersive and localized wave that maintains its shape while traveling at a constant velocity. Unlike periodic waves, a solitary wave is a single pulse or hump that arises typically in nonlinear media and is a solution to certain NPDEs. These waves are characterized by their ability to persist over long distances without changing form. Recently, a special type of solitary wave called a soliton that refers to a wave that maintains its shape while traveling at a constant speed without changing its form or amplitude due to nonlinearity and dispersion canceling each other out has received significant attention [19–21]. When John Scott Russell spotted a lone wave in Scotland's Union Canal in 1834, he made the first note of the soliton phenomena. Unlike ordinary waves, solitons do not disperse over time, they behave as stable, localized pulses that retain their shape and speed. Solitons are particularly interesting because they arise from a balance between dispersive effects and nonlinearity. Solitons are often solutions to NPDEs and appear in many physical contexts, such as fluid dynamics, water waves, and optical fibers. The importance of this subject of research has increased in the last several decades. The nonlinear Schrödinger equation [22–24], Hietarinta equation [25], Gerdgikov-Ivanov equation [26], Fokas system [27], and Biswas-Milovic equation [28] are among the well-known NPDEs that generate solitons.

The focus of this study is on Van der Waals gas system that controls the longitudinal isothermal motion of a compressible fluid in Lagrangian coordinates. This system of two NPDEs is stated as [29]:

$$\begin{aligned} &w_t + \mathbb{P}_x(v) = 0, \\ &v_t - w_x = 0, \end{aligned} \tag{1}$$

where $v = v(x,t)$, $w = w(x,t)$, and $\mathbb{P}(v)$ stand for specific volume, velocity, and pressure, respectively. The viscosity and capillarity effects are taken into account when applying the regularization procedure to (1):

$$\begin{aligned} &w_t + \mathbb{P}_x(v) = \mu w_{xx} - \mu^2 \omega v_{xxx}, \\ &v_t - w_x = 0, \end{aligned} \tag{2}$$

where both μ and $\omega\mu^2$ are positive constants that stand for viscosity and the coefficient of interfacial capillarity (when $\mu, \omega > 0$), respectively. The Van der Waals-like structure is represented by the function $\mathbb{P}(v)$ given below:

$$\mathbb{P}(v) = v(1 - v^2). \tag{3}$$

The Van der Waals system of state is a phenomenological model that describes the behavior of actual gases given the limited size of the gas molecules and intermolecular interactions. While the Van der Waals system was initially created for a three-dimensional system, examining simplified

versions in smaller dimensions may frequently yield important information about the behavior of gases in constrained geometries. To deal with the Van Der Waals modified equation of state and Einstein-Maxwell system, Malaver and Kasmaei [30] also proposed a model that uses an outer Schwarzschild vacuum and interior space-time geometry, while expressing the physical variables in terms of polynomial and basic functions. Physically believable expressions for the mass, density, and radial pressure of heavy pulsars are obtained by analyzing and comparing the model's feasibility with observational data from the Neutron Star Interior Composition Explorer. Kipgen and Singh [31] used the Riemann problem to examine concentration and cavitation processes in order to assess the isothermal Euler equations for van der Waals gas with dust particles in the presence of flux approximation.

Prior to this research work, various other authors have dealt with the Van der Waals system using different methodologies. For instance, Az-Zo'bi used the $e^{-\varphi(\xi)}$-expansion method to find periodic and other solitary wave solutions such as kink wave solutions to the Van der Waals system [32]. Arnous et al. applied three distinct integration schemes, namely the Riccati equations method, enhanced Kudryashov's method, and the Sine-Gordon equation method to the model to find soliton solutions [33]. Sadaf et al. proposed the generalized Kudryashov method and exponential rational function method to seek new exact solution such as periodic, kink, and solitary wave solutions of the Van der Waals normal form for the fluidized granular matter, linked with natural phenomena and industrial applications [34]. Finally, Zafar et al. addressed the Van der Waals normal form for the fluidized matter to establish many new exact solutions using two novel analytical methods namely, the modified Kudryashov method and the hyperbolic function method [35].

Although many researchers have studied solitary wave phenomena in the Van der Waals system in the direction of earlier studies, bright and dark hump and kink structures have not been studied and examined within the framework of the targeted model using RMESEM. This claim reveals a serious gap in the current research, which our study addresses by providing a comprehensive analysis of the model using the recommended RMESEM methodology. The main aims and objectives of the study are as follows: First, a sophisticated wave transformation will transform the intended model into a more manageable system of nonlinear ordinary differential equation (NODEs). Next, assuming a closed-form solution, we will use the RMESEM approach to transform the resultant system of NODEs into an algebraic set of equations. In order to determine the new abundance of solitary wave solutions for the model, the system will ultimately be analytically analyzed using the Maple software. We will conclude by presenting some of the model's kink and hump solitary wave solutions and discussing their effects of free parameters and temporal variation using a combination of two-dimensional visualizations. The efficiency and adaptability of our method in solving a range of nonlinear issues in mathematical science and engineering are validated by our computational research.

The paper is organized as follows: In Section 2, we discuss in detail the proposed RMESEMs working mechanism. We start analyzing the model mathematically in order to determine the NODE in Subsection 3.1. The solutions are then obtained in Subsection 3.2 by utilizing the proposed method. The obtained results have been explained and graphically represented in Section 4. Our conclusions and contributions are finally in Section 5, while the last section provides an appendix.

2. The working mechanism of RMESEM

Numerous analytical methods are based on the Riccati equation. These techniques are useful for researching solitary wave phenomena in various nonlinear models. The proposed method also incorporates the Riccati equation to create and evaluate solitary wave dynamics in the Van der Waals gas system. We describe the mechanism of the RMESEM in this section [11]. Examine the NPDE that follows:

$$L(v, v_t, v_x, v_y, v_z, v_{xx}, v_x v_z \ldots) = 0, \tag{4}$$

where $v = v(t, x, y, ..., z)$. We take the following steps to solve Eq (4).
1) Initially, a variable transformation is carried out as follows:

$$\begin{aligned} &v(t, x, y, ..., z) = V(\phi), \\ &\phi = \omega t \pm \lambda x \pm \mu y \pm ... \pm \nu z. \end{aligned} \tag{5}$$

This transformation converts Eq (4) into the following NODE:

$$Q(V, V', V'', VV', V'V'', \ldots) = 0, \tag{6}$$

where primes are used to denote the derivatives of $V = V(\phi)$ with respect to ϕ.
2) Next, we assume that the NODE in (6) has the following series form solution:

$$V(\phi) = \sum_{l=0}^{\tau} c_l \left(\frac{\xi'(\phi)}{\xi(\phi)}\right)^l + \sum_{l=0}^{\tau-1} w_l \left(\frac{\xi'(\phi)}{\xi(\phi)}\right)^l \cdot \left(\frac{1}{\xi(\phi)}\right), \tag{7}$$

where the parameters $w_l (l = 0, ..., \tau - 1)$ and $c_l (l = 0, ..., \tau)$ stand for the undetermined constants that must be found later, and $\xi(\phi)$ stands for the solution to the resulting Riccati equation:

$$\xi'(\phi) = \varpi + \rho\xi(\phi) + \sigma(\xi(\phi))^2, \tag{8}$$

where ϖ, ρ, and σ are constants.
3) The positive integer τ needed in Eq (7) is then obtained by homogeneously balancing the highest-order derivative and the largest nonlinear term in Eq (6). The homogenous balancing principle is a rule that balance the degree of nonlinear term with the order of dispersion or any other derivative term to provide the appropriate form of the solution ansatz in Eq (7) for the conversion of Eq (6) into a homogenous polynomial. The purpose of balancing is to ensure that the solution ansatz captures the essential behavior of the derivative and nonlinear terms, allowing for an exact solution to be constructed. To satisfy the homogeneous balance requirement, we occasionally integrate Eq (6). To obtain the balance number τ with greater precision, we utilise the subsequent mathematical formulas:

$$D\left(\frac{d^\kappa V}{d\phi^\kappa}\right) = \tau + \kappa, \text{ and } D\left(V^\rho \left(\frac{d^\kappa V}{d\phi^\kappa}\right)^\vartheta\right) = \tau\rho + \vartheta(\kappa + \tau), \tag{9}$$

where D represents the degree of $V(\phi)$ and κ, ρ, and ϑ, are positive integers.
4) Then, all of the terms with the same powers of $\xi(\phi)$ are brought together when Eq (7) is incorporated into Eq (6) or in the equation that emerges from the integration of Eq (6). The result of this process is an equation in terms of $\xi(\phi)$. By setting the coefficients in this equation to zero, an algebraic system

of equations encoding the parameters $c_l(l = 0, ..., \tau)$ and $w_l(l = 0, ..., \tau - 1)$, as well as other related parameters, are generated.
5) Using Maple, the resulting system of nonlinear algebraic equations is analytically evaluated.
6) The values of unknown parameters are then calculated and replaced with $\xi(\phi)$ (Eq (8)'s solution) in Eq (7) in order to create a new multiplicity of solitary wave solutions for Eq (4), which are provided in the pertaining Table 1.

Table 1. Families of solutions $\xi(\phi)$, and $\left(\frac{\xi'(\phi)}{\xi(\phi)}\right)$, where $\epsilon_1, \epsilon_2 \in \mathrm{R}$, $Z = \rho^2 - 4\sigma\varpi$ and $\zeta = \cosh\left(\frac{1}{4}\sqrt{Z}\phi\right)\sinh\left(\frac{1}{4}\sqrt{Z}\phi\right)$.

S. No.	Family	Constraint(s)	$\xi(\phi)$	$\left(\frac{\xi'(\phi)}{\xi(\phi)}\right)$
1	Trigonometric solutions	$Z < 0,\ \sigma \neq 0$	$-\frac{\rho}{2\sigma} + \frac{\sqrt{-Z}\tan\left(\frac{1}{2}\sqrt{-Z}\phi\right)}{2\sigma}$, $-\frac{\rho}{2\sigma} - \frac{\sqrt{-Z}\cot\left(\frac{1}{2}\sqrt{-Z}\phi\right)}{2\sigma}$, $-\frac{\rho}{2\sigma} + \frac{\sqrt{-Z}\left(\tan\left(\sqrt{-Z}\phi\right)+\left(\sec\left(\sqrt{-Z}\phi\right)\right)\right)}{2\sigma}$, $-\frac{\rho}{2\sigma} + \frac{\sqrt{-Z}\left(\tan\left(\sqrt{-Z}\phi\right)-\left(\sec\left(\sqrt{-Z}\phi\right)\right)\right)}{2\sigma}$.	$-\frac{Z\left(1+\left(\tan\left(\frac{1}{2}\sqrt{-Z}\phi\right)\right)^2\right)}{2(-\rho+\sqrt{-Z}\tan\left(\frac{1}{2}\sqrt{-Z}\phi\right))}$, $\frac{\left(1+\left(\cot\left(\frac{1}{2}\sqrt{-Z}\phi\right)\right)^2\right)Z}{2(\rho+\sqrt{-Z}\cot\left(\frac{1}{2}\sqrt{-Z}\phi\right))}$, $\frac{-Z\left(1+\sin\left(\sqrt{-Z}\phi\right)\right)\sec\left(\sqrt{-Z}\phi\right)}{-\rho\cos\left(\sqrt{-Z}\phi\right)+\sqrt{-Z}\sin\left(\sqrt{-Z}\phi\right)+\sqrt{-Z}}$, $\frac{Z\left(\sin\left(\sqrt{-Z}\phi\right)-1\right)\sec\left(\sqrt{-Z}\phi\right)}{-\rho\cos\left(\sqrt{-Z}\phi\right)+\sqrt{-Z}\sin\left(\sqrt{-Z}\phi\right)-\sqrt{-Z}}$.
2	Hyperbolic solutions	$Z > 0,\ \sigma \neq 0$	$-\frac{\rho}{2\sigma} - \frac{\sqrt{Z}\tanh\left(\frac{1}{2}\sqrt{Z}\phi\right)}{2\sigma}$, $-\frac{\rho}{2\sigma} - \frac{\sqrt{Z}\left(\tanh\left(\sqrt{Z}\phi\right)+i\left(\mathrm{sech}\left(\sqrt{Z}\phi\right)\right)\right)}{2\sigma}$, $-\frac{\rho}{2\sigma} - \frac{\sqrt{Z}\left(\tanh\left(\sqrt{Z}\phi\right)-i\left(\mathrm{sech}\left(\sqrt{Z}\phi\right)\right)\right)}{2\sigma}$, $-\frac{\rho}{2\sigma} - \frac{\sqrt{Z}\left(\coth\left(\sqrt{Z}\phi\right)+\left(\mathrm{csch}\left(\sqrt{Z}\phi\right)\right)\right)}{2\sigma}$.	$-\frac{\left(-1+\left(\tanh\left(\frac{1}{2}\sqrt{Z}\phi\right)\right)^2\right)Z}{2(\rho+\sqrt{Z}\tanh\left(\frac{1}{2}\sqrt{Z}\phi\right))}$, $\frac{-Z\left(-1+i\sinh\left(\sqrt{Z}\phi\right)\right)\mathrm{sech}\left(\sqrt{Z}\phi\right)}{\rho\cosh\left(\sqrt{Z}\phi\right)+\sqrt{Z}\sinh\left(\sqrt{Z}\phi\right)+i\sqrt{Z}}$, $\frac{-Z\left(1+i\sinh\left(\sqrt{Z}\phi\right)\right)\mathrm{sech}\left(\sqrt{Z}\phi\right)}{-\rho\cosh\left(\sqrt{Z}\phi\right)-\sqrt{Z}\sinh\left(\sqrt{Z}\phi\right)+i\sqrt{Z}}$, $-\frac{Z\left(2\left(\cosh\left(\frac{1}{4}\sqrt{Z}\phi\right)\right)^2-1\right)}{4\zeta\left(-2\rho\zeta+\sqrt{Z}\right)}$.
3	Rational solutions	$Z = 0$ $Z = 0,\ \&\ \rho = \sigma = 0$ $Z = 0,\ \&\ \rho = \varpi = 0$	$\frac{-2\varpi(\rho\phi+2)}{\rho^2\phi}$, $\phi\,\varpi$, $-\frac{1}{\phi\,\sigma}$.	$\frac{-2}{\phi(\rho\phi+2)}$, $\frac{1}{\phi}$, $-\frac{1}{\phi}$.
4	Exponential solutions	$\sigma = 0,\ \&\ \rho = \chi,\ \varpi = \varsigma\chi$ $\varpi = 0,\ \&\ \rho = \chi,\ \sigma = \varsigma\chi$	$e^{\chi\phi} - \varsigma$, $\frac{e^{\chi\phi}}{1-\varsigma e^{\chi\phi}}$.	$\frac{\chi e^{\chi\phi}}{e^{\chi\phi}-\varsigma}$, $-\frac{\chi}{-1+\varsigma e^{\chi\phi}}$.
5	Rational-Hyperbolic solutions	$\varpi = 0,\ \&\ \rho \neq 0,\ \sigma \neq 0$	$-\frac{\rho\,\epsilon_1}{\sigma(\cosh(\rho\phi)-\sinh(\rho\phi)+\epsilon_2)}$, $-\frac{\rho(\cosh(\rho\phi)+\sinh(\rho\phi))}{\sigma(\cosh(\rho\phi)+\sinh(\rho\phi)+\epsilon_2)}$.	$\frac{\rho(\sinh(\rho\phi)-\cosh(\rho\phi))}{-\cosh(\rho\phi)+\sinh(\rho\phi)-\epsilon_2}$, $\frac{\rho\epsilon_2}{\cosh(\rho\phi)+\sinh(\rho\phi)+\epsilon_2}$.

3. Execution of RMESEM

In order to acquire a variety of solitary wave solutions, including kink-type and hump-type structures, the proposed RMESEM is employed for the under consideration in this section.

3.1. Reduction of the model

When (3) is substituted into (2), the following main framework of the model is deduced:

$$\begin{aligned} &w_t + (v(1-v^2))_x = \mu w_{xx} - \mu^2 \omega v_{xxx}, \\ &v_t - w_x = 0. \end{aligned} \tag{10}$$

We begin with the implementation of the transformation, articulated as follows:

$$\begin{aligned} &v(t,x) = V(\phi), \\ &w(t,x) = W(\phi), \\ &\phi = \lambda(x - st). \end{aligned} \tag{11}$$

This is applied to (10), which yields:

$$\begin{aligned} &-sW' + (\mu\lambda)^2 \omega V''' - \mu\lambda W'' + (V(1-V^2))' = 0, \\ &sV' + W' = 0, \end{aligned} \tag{12}$$

where $V = V(\phi)$ and $W = W(\phi)$. Term by term integrating both the equations in (12) w.r.t ϕ provides:

$$\begin{aligned} &-sW + (\mu\lambda)^2 \omega V'' - \mu\lambda W' + V(1-V^2) = 0, \\ &sV + W = 0. \end{aligned} \tag{13}$$

The second equation in (13) implies $W = -sV$, which reduces the entire system to the ensuing single NODE by substitution:

$$s^2 V + (\mu\lambda)^2 \omega V'' + \mu\lambda s V' + V(1-V^2) + \Omega = 0, \tag{14}$$

where Ω signifies the constant of integration.

3.2. Novel families of soliton solutions

By establishing the homogenous balancing principle between V'' and V^3 given in (14) and using the formula in (9) we get $\tau = 1$. The following closed form solution is proposed by RMESEM for (14) when we substitute $\tau = 1$ in (7):

$$V(\phi) = c_0 + c_1 \left(\frac{\xi'(\phi)}{\xi(\phi)} \right) + \frac{w_0}{\xi(\phi)}, \tag{15}$$

where the arbitrary constants c_0, c_1, and w_0 need estimation. Putting (15) into (14) and gathering all the terms with the same power of $\xi(\phi)$ yields an expression in $\xi(\phi)$. Setting all the coefficients of the expression to zero results in a system of algebraic equations. The resultant problem is solved using

Maple to get the following three cases of solutions for the relevant parameters.

Case 1.

$$c_0 = \frac{3\rho w_0 - \Phi}{6\varpi}, c_1 = 0, w_0 = w_0, s = s, \lambda = \frac{\Phi w_0}{2s\mu\varpi^2}, \omega = \frac{2\varpi^2 s^2}{12\varpi^2(s^2+1) - 3Z{w_0}^2}, \Omega = \frac{\Phi\left(\varpi^2\left(s^2+1\right) - Z{w_0}^2\right)}{9\varpi^3}. \quad (16)$$

Case 2.

$$c_0 = \frac{-\rho}{\sqrt{8\varpi\sigma+\rho^2}}, c_1 = \frac{2}{\sqrt{8\varpi\sigma+\rho^2}}, w_0 = 0, s = 0, \lambda = \lambda, \omega = \frac{2}{(8\varpi\sigma+\rho^2)\lambda^2\mu^2}, \Omega = \frac{8\varpi\rho\sigma}{(8\varpi\sigma+\rho^2)^{3/2}}. \quad (17)$$

Case 3.

$$c_0 = -\frac{1}{2}\rho c_1 + \frac{1}{6}\Psi, c_1 = c_1, w_0 = -\varpi c_1, s = s, \lambda = \frac{\Psi c_1}{2s\mu}, \omega = \frac{2s^2}{\Psi^2}, \Omega = -\frac{\Psi\left(-Z{c_1}^2 + s^2 + 1\right)}{9}. \quad (18)$$

Here

$$\Phi = \sqrt{12\varpi^2(s^2+1) - 3Z{w_0}^2},$$
$$\Psi = \sqrt{-3Z{c_1}^2 + 12s^2 + 12},$$
$$Z = \rho^2 - 4\sigma\varpi.$$

Considering Case 1 and using (11) and (15) with the corresponding solutions of (8) stated in Table 1, we construct the subsequent new families of solitary wave solutions for the Van der Waals system given in (10).

Solution Set. 1.1: When $Z < 0,\ \sigma \neq 0$,

$$\begin{aligned} v_{1,1}(t,x) &= \left(-\frac{1}{2}\frac{\rho}{\sigma} + \frac{1}{2}\frac{\sqrt{-Z}\tan\left(\frac{1}{2}\sqrt{-Z}\phi\right)}{\sigma}\right)w_0 - \frac{1}{6}\frac{-3\rho w_0 + \Phi}{\varpi}, \\ w_{1,1}(t,x) &= -s\left(\left(-\frac{1}{2}\frac{\rho}{\sigma} + \frac{1}{2}\frac{\sqrt{-Z}\tan\left(\frac{1}{2}\sqrt{-Z}\phi\right)}{\sigma}\right)w_0 - \frac{1}{6}\frac{-3\rho w_0 + \Phi}{\varpi}\right), \end{aligned} \quad (19)$$

$$\begin{aligned} v_{1,2}(t,x) &= \left(-\frac{1}{2}\frac{\rho}{\sigma} - \frac{1}{2}\frac{\sqrt{-Z}\cot\left(\frac{1}{2}\sqrt{-Z}\phi\right)}{\sigma}\right)w_0 - \frac{1}{6}\frac{-3\rho w_0 + \Phi}{\varpi}, \\ w_{1,2}(t,x) &= -s\left(\left(-\frac{1}{2}\frac{\rho}{\sigma} - \frac{1}{2}\frac{\sqrt{-Z}\cot\left(\frac{1}{2}\sqrt{-Z}\phi\right)}{\sigma}\right)w_0 - \frac{1}{6}\frac{-3\rho w_0 + \Phi}{\varpi}\right), \end{aligned} \quad (20)$$

$$\begin{aligned} v_{1,3}(t,x) &= \left(-\frac{1}{2}\frac{\rho}{\sigma} + \frac{1}{2}\frac{\sqrt{-Z}\left(\tan\left(\sqrt{-Z}\phi\right) + \sec\left(\sqrt{-Z}\phi\right)\right)}{\sigma}\right)w_0 - \frac{1}{6}\frac{-3\rho w_0 + \Phi}{\varpi}, \\ w_{1,3}(t,x) &= -s\left(\left(-\frac{1}{2}\frac{\rho}{\sigma} + \frac{1}{2}\frac{\sqrt{-Z}\left(\tan\left(\sqrt{-Z}\phi\right) + \sec\left(\sqrt{-Z}\phi\right)\right)}{\sigma}\right)w_0 - \frac{1}{6}\frac{-3\rho w_0 + \Phi}{\varpi}\right), \end{aligned} \quad (21)$$

and

$$v_{1,4}(t,x) = \left(-\frac{1}{2}\frac{\rho}{\sigma} + \frac{1}{2}\frac{\sqrt{-Z}\left(\tan\left(\sqrt{-Z}\phi\right) - \sec\left(\sqrt{-Z}\phi\right)\right)}{\sigma}\right)w_0 - \frac{1}{6}\frac{-3\rho w_0 + \Phi}{\varpi},$$
$$w_{1,4}(t,x) = -s\left(\left(-\frac{1}{2}\frac{\rho}{\sigma} + \frac{1}{2}\frac{\sqrt{-Z}\left(\tan\left(\sqrt{-Z}\phi\right) - \sec\left(\sqrt{-Z}\phi\right)\right)}{\sigma}\right)w_0 - \frac{1}{6}\frac{-3\rho w_0 + \Phi}{\varpi}\right). \tag{22}$$

Solution Set. 1.2: When $Z > 0,\ \sigma \neq 0$,

$$v_{1,5}(t,x) = \left(-\frac{1}{2}\frac{\rho}{\sigma} - \frac{1}{2}\frac{\sqrt{Z}\tanh\left(\frac{1}{2}\sqrt{Z}\phi\right)}{\sigma}\right)w_0 - \frac{1}{6}\frac{-3\rho w_0 + \Phi}{\varpi},$$
$$w_{1,5}(t,x) = -s\left(\left(-\frac{1}{2}\frac{\rho}{\sigma} - \frac{1}{2}\frac{\sqrt{Z}\tanh\left(\frac{1}{2}\sqrt{Z}\phi\right)}{\sigma}\right)w_0 - \frac{1}{6}\frac{-3\rho w_0 + \Phi}{\varpi}\right), \tag{23}$$

$$v_{1,6}(t,x) = \left(-\frac{1}{2}\frac{\rho}{\sigma} - \frac{1}{2}\frac{\sqrt{Z}\left(\tanh\left(\sqrt{Z}\phi\right) + i\mathrm{sech}\left(\sqrt{Z}\phi\right)\right)}{\sigma}\right)w_0 - \frac{1}{6}\frac{-3\rho w_0 + \Phi}{\varpi},$$
$$w_{1,6}(t,x) = -s\left(\left(-\frac{1}{2}\frac{\rho}{\sigma} - \frac{1}{2}\frac{\sqrt{Z}\left(\tanh\left(\sqrt{Z}\phi\right) + i\mathrm{sech}\left(\sqrt{Z}\phi\right)\right)}{\sigma}\right)w_0 - \frac{1}{6}\frac{-3\rho w_0 + \Phi}{\varpi}\right), \tag{24}$$

$$v_{1,7}(t,x) = \left(-\frac{1}{2}\frac{\rho}{\sigma} - \frac{1}{2}\frac{\sqrt{Z}\left(\tanh\left(\sqrt{Z}\phi\right) - i\mathrm{sech}\left(\sqrt{Z}\phi\right)\right)}{\sigma}\right)w_0 - \frac{1}{6}\frac{-3\rho w_0 + \Phi}{\varpi},$$
$$w_{1,7}(t,x) = -s\left(\left(-\frac{1}{2}\frac{\rho}{\sigma} - \frac{1}{2}\frac{\sqrt{Z}\left(\tanh\left(\sqrt{Z}\phi\right) - i\mathrm{sech}\left(\sqrt{Z}\phi\right)\right)}{\sigma}\right)w_0 - \frac{1}{6}\frac{-3\rho w_0 + \Phi}{\varpi}\right), \tag{25}$$

and

$$v_{1,8}(t,x) = \left(-\frac{1}{2}\frac{\rho}{\sigma} - \frac{1}{4}\frac{\sqrt{Z}\left(\tanh\left(\frac{1}{4}\sqrt{Z}\phi\right) - \coth\left(\frac{1}{4}\sqrt{Z}\phi\right)\right)}{\sigma}\right)w_0 - \frac{1}{6}\frac{-3\rho w_0 + \Phi}{\varpi},$$
$$w_{1,8}(t,x) = -s\left(\left(-\frac{1}{2}\frac{\rho}{\sigma} - \frac{1}{4}\frac{\sqrt{Z}\left(\tanh\left(\frac{1}{4}\sqrt{Z}\phi\right) - \coth\left(\frac{1}{4}\sqrt{Z}\phi\right)\right)}{\sigma}\right)w_0 - \frac{1}{6}\frac{-3\rho w_0 + \Phi}{\varpi}\right). \tag{26}$$

Solution Set. 1.3: When $Z = 0$,

$$v_{1,9}(t,x) = -\frac{1}{6}\frac{12\,\varpi^2\phi\rho\,w_0 + 2\,\varpi\sqrt{3\,(s^2+1)}\phi\rho^2 - 3\,\phi\rho^3 w_0 + 24\,\varpi^2 w_0}{\rho^2\phi\,\varpi},$$
$$w_{1,9}(t,x) = -s\left(-\frac{1}{6}\frac{12\,\varpi^2\phi\rho\,w_0 + 2\,\varpi\sqrt{3\,(s^2+1)}\phi\rho^2 - 3\,\phi\rho^3 w_0 + 24\,\varpi^2 w_0}{\rho^2\phi\,\varpi}\right). \tag{27}$$

Solution Set. 1.4: When $Z = 0$ such that $\rho = 0$ and $\sigma = 0$,

$$v_{1,10}(t,x) = \frac{1}{6}\frac{6\,\varpi^2\phi\,w_0 - \sqrt{12\,\varpi^2 s^2 + 12\,\varpi^2}}{\varpi},$$
$$w_{1,10}(t,x) = -s\left(\frac{1}{6}\frac{6\,\varpi^2\phi\,w_0 - \sqrt{12\,\varpi^2 s^2 + 12\,\varpi^2}}{\varpi}\right). \tag{28}$$

Solution Set. 1.5: When $\rho = \chi$, $\varpi = \varsigma\chi(\varsigma \neq 0)$, and $\sigma = 0$,

$$\begin{aligned} v_{1,11}(t,x) =& \frac{1}{6}\,\frac{6\,w_0\varsigma\chi\,\mathrm{e}^{\chi\phi} - 6\,w_0\varsigma^2\chi + 3\chi\,w_0 - \sqrt{12\chi^2 s^2\varsigma^2 + 12\,\varsigma^2\chi^2 - 3\chi^2 {w_0}^2}}{\varsigma\chi}, \\ w_{1,11}(t,x) =& -s\Big(\frac{1}{6}\,\frac{6\,w_0\varsigma\chi\,\mathrm{e}^{\chi\phi} - 6\,w_0\varsigma^2\chi + 3\chi\,w_0 - \sqrt{12\chi^2 s^2\varsigma^2 + 12\,\varsigma^2\chi^2 - 3\chi^2 {w_0}^2}}{\varsigma\chi}\Big). \end{aligned} \tag{29}$$

Where $\phi = \frac{\Phi\, w_0}{2s\mu\,\varpi^2}(x - st)$ in the above solutions of Case 1.

Considering Case 2 and using (11) and (15) with the corresponding solutions of (8) stated in Table 1, we construct the subsequent new families of solitary wave solutions for the Van der Waals system given in (10):

Solution Set. 2.1: When $Z < 0,\ \sigma \neq 0$,

$$\begin{aligned} v_{2,1}(t,x) =& -\frac{Z\left(1 + \left(\tan\left(\frac{1}{2}\,\sqrt{-Z}\phi\right)\right)^2\right)}{\left(\sqrt{-Z}\tan\left(\frac{1}{2}\,\sqrt{-Z}\phi\right) - \rho\right)\sqrt{8\,\varpi\,\sigma + \rho^2}} - \frac{\rho}{\sqrt{8\,\varpi\,\sigma + \rho^2}}, \\ w_{2,1}(t,x) =& -s\Big(-\frac{Z\left(1 + \left(\tan\left(\frac{1}{2}\,\sqrt{-Z}\phi\right)\right)^2\right)}{\left(\sqrt{-Z}\tan\left(\frac{1}{2}\,\sqrt{-Z}\phi\right) - \rho\right)\sqrt{8\,\varpi\,\sigma + \rho^2}} - \frac{\rho}{\sqrt{8\,\varpi\,\sigma + \rho^2}}\Big), \end{aligned} \tag{30}$$

$$\begin{aligned} v_{2,2}(t,x) =& \frac{Z\left(\left(\cot\left(\frac{1}{2}\,\sqrt{-Z}\phi\right)\right)^2 + 1\right)}{\left(\sqrt{-Z}\cot\left(\frac{1}{2}\,\sqrt{-Z}\phi\right) + \rho\right)\sqrt{8\,\varpi\,\sigma + \rho^2}} - \frac{\rho}{\sqrt{8\,\varpi\,\sigma + \rho^2}}, \\ w_{2,2}(t,x) =& -s\Big(\frac{Z\left(\left(\cot\left(\frac{1}{2}\,\sqrt{-Z}\phi\right)\right)^2 + 1\right)}{\left(\sqrt{-Z}\cot\left(\frac{1}{2}\,\sqrt{-Z}\phi\right) + \rho\right)\sqrt{8\,\varpi\,\sigma + \rho^2}} - \frac{\rho}{\sqrt{8\,\varpi\,\sigma + \rho^2}}\Big), \end{aligned} \tag{31}$$

$$\begin{aligned} v_{2,3}(t,x) =& -2\,\frac{Z\left(1 + \sin\left(\sqrt{-Z}\phi\right)\right)}{\cos\left(\sqrt{-Z}\phi\right)\left(\sqrt{-Z}\sin\left(\sqrt{-Z}\phi\right) - \rho\,\cos\left(\sqrt{-Z}\phi\right) + \sqrt{-Z}\right)\sqrt{8\,\varpi\,\sigma + \rho^2}} - \frac{\rho}{\sqrt{8\,\varpi\,\sigma + \rho^2}}, \\ w_{2,3}(t,x) =& -s\Big(-2\,\frac{Z\left(1 + \sin\left(\sqrt{-Z}\phi\right)\right)}{\cos\left(\sqrt{-Z}\phi\right)\left(\sqrt{-Z}\sin\left(\sqrt{-Z}\phi\right) - \rho\,\cos\left(\sqrt{-Z}\phi\right) + \sqrt{-Z}\right)\sqrt{8\,\varpi\,\sigma + \rho^2}} - \frac{\rho}{\sqrt{8\,\varpi\,\sigma + \rho^2}}\Big), \end{aligned} \tag{32}$$

and

$$\begin{aligned} v_{2,4}(t,x) =& 2\,\frac{Z\left(\sin\left(\sqrt{-Z}\phi\right) - 1\right)}{\cos\left(\sqrt{-Z}\phi\right)\left(\sqrt{-Z}\sin\left(\sqrt{-Z}\phi\right) - \rho\,\cos\left(\sqrt{-Z}\phi\right) - \sqrt{-Z}\right)\sqrt{8\,\varpi\,\sigma + \rho^2}} - \frac{\rho}{\sqrt{8\,\varpi\,\sigma + \rho^2}}, \\ w_{2,4}(t,x) =& -s\Big(2\,\frac{Z\left(\sin\left(\sqrt{-Z}\phi\right) - 1\right)}{\cos\left(\sqrt{-Z}\phi\right)\left(\sqrt{-Z}\sin\left(\sqrt{-Z}\phi\right) - \rho\,\cos\left(\sqrt{-Z}\phi\right) - \sqrt{-Z}\right)\sqrt{8\,\varpi\,\sigma + \rho^2}} - \frac{\rho}{\sqrt{8\,\varpi\,\sigma + \rho^2}}\Big). \end{aligned} \tag{33}$$

Solution Set. 2.2: When $Z > 0,\ \sigma \neq 0$,

$$\begin{aligned} v_{2,5}(t,x) =& -\frac{Z\left(\left(\tanh\left(\frac{1}{2}\ \sqrt{Z}\phi\right)\right)^2-1\right)}{\left(\sqrt{Z}\tanh\left(\frac{1}{2}\ \sqrt{Z}\phi\right)+\rho\right)\sqrt{8\,\varpi\,\sigma+\rho^2}}-\frac{\rho}{\sqrt{8\,\varpi\,\sigma+\rho^2}},\\ w_{2,5}(t,x) =& -s\Bigg(-\frac{Z\left(\left(\tanh\left(\frac{1}{2}\ \sqrt{Z}\phi\right)\right)^2-1\right)}{\left(\sqrt{Z}\tanh\left(\frac{1}{2}\ \sqrt{Z}\phi\right)+\rho\right)\sqrt{8\,\varpi\,\sigma+\rho^2}}-\frac{\rho}{\sqrt{8\,\varpi\,\sigma+\rho^2}}\Bigg), \end{aligned} \tag{34}$$

$$v_{2,6}(t,x) = -2\,\frac{Z\left(i\sinh\left(\sqrt{Z}\phi\right)-1\right)}{\cosh\left(\sqrt{Z}\phi\right)\left(i\sqrt{Z}+\sqrt{Z}\sinh\left(\sqrt{Z}\phi\right)+\rho\,\cosh\left(\sqrt{Z}\phi\right)\right)\sqrt{8\,\varpi\,\sigma+\rho^2}}-\frac{\rho}{\sqrt{8\,\varpi\,\sigma+\rho^2}},$$

$$w_{2,6}(t,x) = -s\Bigg(-2\,\frac{Z\left(i\sinh\left(\sqrt{Z}\phi\right)-1\right)}{\cosh\left(\sqrt{Z}\phi\right)\left(i\sqrt{Z}+\sqrt{Z}\sinh\left(\sqrt{Z}\phi\right)+\rho\,\cosh\left(\sqrt{Z}\phi\right)\right)\sqrt{8\,\varpi\,\sigma+\rho^2}}-\frac{\rho}{\sqrt{8\,\varpi\,\sigma+\rho^2}}\Bigg), \tag{35}$$

$$v_{2,7}(t,x) = -2\,\frac{Z\left(i\sinh\left(\sqrt{Z}\phi\right)+1\right)}{\cosh\left(\sqrt{Z}\phi\right)\left(i\sqrt{Z}-\sqrt{Z}\sinh\left(\sqrt{Z}\phi\right)-\rho\,\cosh\left(\sqrt{Z}\phi\right)\right)\sqrt{8\,\varpi\,\sigma+\rho^2}}-\frac{\rho}{\sqrt{8\,\varpi\,\sigma+\rho^2}},$$

$$w_{2,7}(t,x) = -s\Bigg(-2\,\frac{Z\left(i\sinh\left(\sqrt{Z}\phi\right)+1\right)}{\cosh\left(\sqrt{Z}\phi\right)\left(i\sqrt{Z}-\sqrt{Z}\sinh\left(\sqrt{Z}\phi\right)-\rho\,\cosh\left(\sqrt{Z}\phi\right)\right)\sqrt{8\,\varpi\,\sigma+\rho^2}}-\frac{\rho}{\sqrt{8\,\varpi\,\sigma+\rho^2}}\Bigg), \tag{36}$$

and

$$\begin{aligned} v_{2,8}(t,x) =& -\frac{1}{2}\,\frac{Z\left(2\left(\cosh\left(\frac{1}{4}\ \sqrt{Z}\phi\right)\right)^2-1\right)}{\zeta\left(-2\rho\,\zeta+\sqrt{Z}\right)\sqrt{8\,\varpi\,\sigma+\rho^2}}-\frac{\rho}{\sqrt{8\,\varpi\,\sigma+\rho^2}},\\ w_{2,8}(t,x) =& -s\Bigg(-\frac{1}{2}\,\frac{Z\left(2\left(\cosh\left(\frac{1}{4}\ \sqrt{Z}\phi\right)\right)^2-1\right)}{\zeta\left(-2\rho\,\zeta+\sqrt{Z}\right)\sqrt{8\,\varpi\,\sigma+\rho^2}}-\frac{\rho}{\sqrt{8\,\varpi\,\sigma+\rho^2}}\Bigg). \end{aligned} \tag{37}$$

Solution Set. 2.3: When $Z = 0$,

$$\begin{aligned} v_{2,9}(t,x) =& -4\,\frac{1}{\phi\ (\rho\,\phi+2)\ \sqrt{8\,\varpi\,\sigma+\rho^2}}-\frac{\rho}{\sqrt{8\,\varpi\,\sigma+\rho^2}},\\ w_{2,9}(t,x) =& -s\Bigg(-4\,\frac{1}{\phi\ (\rho\,\phi+2)\ \sqrt{8\,\varpi\,\sigma+\rho^2}}-\frac{\rho}{\sqrt{8\,\varpi\,\sigma+\rho^2}}\Bigg). \end{aligned} \tag{38}$$

Solution Set. 2.5: When $\rho = \chi$, $\varpi = \varsigma\chi(\varsigma \neq 0)$, and $\sigma = 0$,

$$\begin{aligned} v_{2,11}(t,x) =& \frac{\mathrm{csgn}\,(\chi)\,(\mathrm{e}^{\chi\,\phi}+\varsigma)}{\mathrm{e}^{\chi\,\phi}-\varsigma},\\ w_{2,11}(t,x) =& -s\Bigg(\frac{\mathrm{csgn}\,(\chi)\,(\mathrm{e}^{\chi\,\phi}+\varsigma)}{\mathrm{e}^{\chi\,\phi}-\varsigma}\Bigg). \end{aligned} \tag{39}$$

Solution Set. 2.6: When $\rho = \chi$, $\sigma = \varsigma\chi(\varsigma \neq 0)$, and $\varpi = 0$,

$$\begin{aligned} v_{2,12}(t,x) &= -\frac{\operatorname{csgn}(\chi)\,(\varsigma\,\mathrm{e}^{\chi\,\phi}+1)}{-1+\varsigma\,\mathrm{e}^{\chi\,\phi}}, \\ w_{2,12}(t,x) &= -s\Big(-\frac{\operatorname{csgn}(\chi)\,(\varsigma\,\mathrm{e}^{\chi\,\phi}+1)}{-1+\varsigma\,\mathrm{e}^{\chi\,\phi}}\Big). \end{aligned} \tag{40}$$

Solution Set. 2.7: When $\rho \neq 0$, $\sigma \neq 0$, and $\varpi = 0$,

$$\begin{aligned} v_{2,13}(t,x) &= \frac{(\sinh(\rho\,\phi)-\cosh(\rho\,\phi)+\epsilon_2)\operatorname{csgn}(\rho)}{\sinh(\rho\,\phi)-\cosh(\rho\,\phi)-\epsilon_2}, \\ w_{2,13}(t,x) &= -s\Big(\frac{(\sinh(\rho\,\phi)-\cosh(\rho\,\phi)+\epsilon_2)\operatorname{csgn}(\rho)}{\sinh(\rho\,\phi)-\cosh(\rho\,\phi)-\epsilon_2}\Big), \end{aligned} \tag{41}$$

and

$$\begin{aligned} v_{2,14}(t,x) &= -\frac{(-\epsilon_2+\cosh(\rho\,\phi)+\sinh(\rho\,\phi))\operatorname{csgn}(\rho)}{\cosh(\rho\,\phi)+\sinh(\rho\,\phi)+\epsilon_2}, \\ w_{2,14}(t,x) &= -s\Big(-\frac{(-\epsilon_2+\cosh(\rho\,\phi)+\sinh(\rho\,\phi))\operatorname{csgn}(\rho)}{\cosh(\rho\,\phi)+\sinh(\rho\,\phi)+\epsilon_2}\Big). \end{aligned} \tag{42}$$

$\phi = \lambda x$ in the above solutions of Case 2.

Considering Case 3 and using (11) and (15) with the corresponding solutions of (8) stated in Table 1, we construct the subsequent new families of solitary wave solutions for the Van der Waals system given in (10).

Solution Set. 3.1: When $Z < 0,\ \sigma \neq 0$,

$$\begin{aligned} v_{3,1}(t,x) &= -\left(-\frac{1}{2}\frac{\rho}{\sigma}+\frac{1}{2}\frac{\sqrt{-Z}\tan\left(\frac{1}{2}\sqrt{-Z}\phi\right)}{\sigma}\right)\varpi\,c_1-\frac{1}{2}\frac{Z\left(1+\left(\tan\left(\frac{1}{2}\sqrt{-Z}\phi\right)\right)^2\right)c_1}{\sqrt{-Z}\tan\left(\frac{1}{2}\sqrt{-Z}\phi\right)-\rho}-\frac{1}{2}\rho\,c_1+\frac{1}{6}\Psi, \\ w_{3,1}(t,x) &= -s\Big(-\left(-\frac{1}{2}\frac{\rho}{\sigma}+\frac{1}{2}\frac{\sqrt{-Z}\tan\left(\frac{1}{2}\sqrt{-Z}\phi\right)}{\sigma}\right)\varpi\,c_1-\frac{1}{2}\frac{Z\left(1+\left(\tan\left(\frac{1}{2}\sqrt{-Z}\phi\right)\right)^2\right)c_1}{\sqrt{-Z}\tan\left(\frac{1}{2}\sqrt{-Z}\phi\right)-\rho}-\frac{1}{2}\rho\,c_1+\frac{1}{6}\Psi\Big), \end{aligned} \tag{43}$$

$$\begin{aligned} v_{3,2}(t,x) &= -\left(-\frac{1}{2}\frac{\rho}{\sigma}-\frac{1}{2}\frac{\sqrt{-Z}\cot\left(\frac{1}{2}\sqrt{-Z}\phi\right)}{\sigma}\right)\varpi\,c_1+\frac{1}{2}\frac{Z\left(\left(\cot\left(\frac{1}{2}\sqrt{-Z}\phi\right)\right)^2+1\right)c_1}{\sqrt{-Z}\cot\left(\frac{1}{2}\sqrt{-Z}\phi\right)+\rho}-\frac{1}{2}\rho\,c_1+\frac{1}{6}\Psi, \\ w_{3,2}(t,x) &= -s\Big(-\left(-\frac{1}{2}\frac{\rho}{\sigma}-\frac{1}{2}\frac{\sqrt{-Z}\cot\left(\frac{1}{2}\sqrt{-Z}\phi\right)}{\sigma}\right)\varpi\,c_1+\frac{1}{2}\frac{Z\left(\left(\cot\left(\frac{1}{2}\sqrt{-Z}\phi\right)\right)^2+1\right)c_1}{\sqrt{-Z}\cot\left(\frac{1}{2}\sqrt{-Z}\phi\right)+\rho}-\frac{1}{2}\rho\,c_1+\frac{1}{6}\Psi\Big), \end{aligned} \tag{44}$$

$$
\begin{aligned}
v_{3,3}(t,x) =& -\left(-\frac{1}{2}\frac{\rho}{\sigma}+\frac{1}{2}\frac{\sqrt{-Z}\left(\tan\left(\sqrt{-Z}\phi\right)+\sec\left(\sqrt{-Z}\phi\right)\right)}{\sigma}\right)\varpi\, c_1\\
&-\frac{Z\left(1+\sin\left(\sqrt{-Z}\phi\right)\right)c_1}{\cos\left(\sqrt{-Z}\phi\right)\left(\sqrt{-Z}\sin\left(\sqrt{-Z}\phi\right)-\rho\,\cos\left(\sqrt{-Z}\phi\right)+\sqrt{-Z}\right)}-\frac{1}{2}\rho\, c_1+\frac{1}{6}\Psi,\\
w_{3,3}(t,x) =& -s\Bigg(-\left(-\frac{1}{2}\frac{\rho}{\sigma}+\frac{1}{2}\frac{\sqrt{-Z}\left(\tan\left(\sqrt{-Z}\phi\right)+\sec\left(\sqrt{-Z}\phi\right)\right)}{\sigma}\right)\varpi\, c_1\\
&-\frac{Z\left(1+\sin\left(\sqrt{-Z}\phi\right)\right)c_1}{\cos\left(\sqrt{-Z}\phi\right)\left(\sqrt{-Z}\sin\left(\sqrt{-Z}\phi\right)-\rho\,\cos\left(\sqrt{-Z}\phi\right)+\sqrt{-Z}\right)}-\frac{1}{2}\rho\, c_1+\frac{1}{6}\Psi\Bigg),
\end{aligned}
\tag{45}
$$

and

$$
\begin{aligned}
v_{3,4}(t,x) =& -\left(-\frac{1}{2}\frac{\rho}{\sigma}+\frac{1}{2}\frac{\sqrt{-Z}\left(\tan\left(\sqrt{-Z}\phi\right)-\sec\left(\sqrt{-Z}\phi\right)\right)}{\sigma}\right)\varpi\, c_1\\
&+\frac{Z\left(\sin\left(\sqrt{-Z}\phi\right)-1\right)c_1}{\cos\left(\sqrt{-Z}\phi\right)\left(\sqrt{-Z}\sin\left(\sqrt{-Z}\phi\right)-\rho\,\cos\left(\sqrt{-Z}\phi\right)-\sqrt{-Z}\right)}-\frac{1}{2}\rho\, c_1+\frac{1}{6}\Psi,\\
w_{3,4}(t,x) =& -s\Bigg(-\left(-\frac{1}{2}\frac{\rho}{\sigma}+\frac{1}{2}\frac{\sqrt{-Z}\left(\tan\left(\sqrt{-Z}\phi\right)-\sec\left(\sqrt{-Z}\phi\right)\right)}{\sigma}\right)\varpi\, c_1\\
&+\frac{Z\left(\sin\left(\sqrt{-Z}\phi\right)-1\right)c_1}{\cos\left(\sqrt{-Z}\phi\right)\left(\sqrt{-Z}\sin\left(\sqrt{-Z}\phi\right)-\rho\,\cos\left(\sqrt{-Z}\phi\right)-\sqrt{-Z}\right)}-\frac{1}{2}\rho\, c_1+\frac{1}{6}\Psi\Bigg).
\end{aligned}
\tag{46}
$$

Solution Set. 3.2: When $Z>0,\ \sigma\neq 0$,

$$
\begin{aligned}
v_{3,5}(t,x) =& -\left(-\frac{1}{2}\frac{\rho}{\sigma}-\frac{1}{2}\frac{\sqrt{Z}\tanh\left(\frac{1}{2}\sqrt{Z}\phi\right)}{\sigma}\right)\varpi\, c_1-\frac{1}{2}\frac{Z\left(\left(\tanh\left(\frac{1}{2}\sqrt{Z}\phi\right)\right)^2-1\right)c_1}{\sqrt{Z}\tanh\left(\frac{1}{2}\sqrt{Z}\phi\right)+\rho}-\frac{1}{2}\rho\, c_1+\frac{1}{6}\Psi,\\
w_{3,5}(t,x) =& -s\Bigg(-\left(-\frac{1}{2}\frac{\rho}{\sigma}-\frac{1}{2}\frac{\sqrt{Z}\tanh\left(\frac{1}{2}\sqrt{Z}\phi\right)}{\sigma}\right)\varpi\, c_1-\frac{1}{2}\frac{Z\left(\left(\tanh\left(\frac{1}{2}\sqrt{Z}\phi\right)\right)^2-1\right)c_1}{\sqrt{Z}\tanh\left(\frac{1}{2}\sqrt{Z}\phi\right)+\rho}-\frac{1}{2}\rho\, c_1+\frac{1}{6}\Psi\Bigg),
\end{aligned}
\tag{47}
$$

$$
\begin{aligned}
v_{3,6}(t,x) =& -\left(-\frac{1}{2}\frac{\rho}{\sigma}-\frac{1}{2}\frac{\sqrt{Z}\left(\tanh\left(\sqrt{Z}\phi\right)+i\operatorname{sech}\left(\sqrt{Z}\phi\right)\right)}{\sigma}\right)\varpi\, c_1\\
&-\frac{Z\left(i\sinh\left(\sqrt{Z}\phi\right)-1\right)c_1}{\cosh\left(\sqrt{Z}\phi\right)\left(i\sqrt{Z}+\sqrt{Z}\sinh\left(\sqrt{Z}\phi\right)+\rho\cosh\left(\sqrt{Z}\phi\right)\right)}-\frac{1}{2}\rho\, c_1+\frac{1}{6}\Psi,\\
w_{3,6}(t,x) =& -s\Bigg(-\left(-\frac{1}{2}\frac{\rho}{\sigma}-\frac{1}{2}\frac{\sqrt{Z}\left(\tanh\left(\sqrt{Z}\phi\right)+i\operatorname{sech}\left(\sqrt{Z}\phi\right)\right)}{\sigma}\right)\varpi\, c_1\\
&-\frac{Z\left(i\sinh\left(\sqrt{Z}\phi\right)-1\right)c_1}{\cosh\left(\sqrt{Z}\phi\right)\left(i\sqrt{Z}+\sqrt{Z}\sinh\left(\sqrt{Z}\phi\right)+\rho\cosh\left(\sqrt{Z}\phi\right)\right)}-\frac{1}{2}\rho\, c_1+\frac{1}{6}\Psi\Bigg),\\
v_{3,7}(t,x) =& -\left(-\frac{1}{2}\frac{\rho}{\sigma}-\frac{1}{2}\frac{\sqrt{Z}\left(\tanh\left(\sqrt{Z}\phi\right)-i\operatorname{sech}\left(\sqrt{Z}\phi\right)\right)}{\sigma}\right)\varpi\, c_1\\
&-\frac{Z\left(i\sinh\left(\sqrt{Z}\phi\right)+1\right)c_1}{\cosh\left(\sqrt{Z}\phi\right)\left(i\sqrt{Z}-\sqrt{Z}\sinh\left(\sqrt{Z}\phi\right)-\rho\cosh\left(\sqrt{Z}\phi\right)\right)}-\frac{1}{2}\rho\, c_1+\frac{1}{6}\Psi,\\
w_{3,7}(t,x) =& -s\Bigg(-\left(-\frac{1}{2}\frac{\rho}{\sigma}-\frac{1}{2}\frac{\sqrt{Z}\left(\tanh\left(\sqrt{Z}\phi\right)-i\operatorname{sech}\left(\sqrt{Z}\phi\right)\right)}{\sigma}\right)\varpi\, c_1\\
&-\frac{Z\left(i\sinh\left(\sqrt{Z}\phi\right)+1\right)c_1}{\cosh\left(\sqrt{Z}\phi\right)\left(i\sqrt{Z}-\sqrt{Z}\sinh\left(\sqrt{Z}\phi\right)-\rho\cosh\left(\sqrt{Z}\phi\right)\right)}-\frac{1}{2}\rho\, c_1+\frac{1}{6}\Psi\Bigg),
\end{aligned}
\tag{48}
$$

$$
\begin{aligned}
v_{3,7}(t,x) =& -\left(-\frac{1}{2}\frac{\rho}{\sigma}-\frac{1}{2}\frac{\sqrt{Z}\left(\tanh\left(\sqrt{Z}\phi\right)-i\operatorname{sech}\left(\sqrt{Z}\phi\right)\right)}{\sigma}\right)\varpi\, c_1\\
&-\frac{Z\left(i\sinh\left(\sqrt{Z}\phi\right)+1\right)c_1}{\cosh\left(\sqrt{Z}\phi\right)\left(i\sqrt{Z}-\sqrt{Z}\sinh\left(\sqrt{Z}\phi\right)-\rho\cosh\left(\sqrt{Z}\phi\right)\right)}-\frac{1}{2}\rho\, c_1+\frac{1}{6}\Psi,\\
w_{3,7}(t,x) =& -s\Bigg(-\left(-\frac{1}{2}\frac{\rho}{\sigma}-\frac{1}{2}\frac{\sqrt{Z}\left(\tanh\left(\sqrt{Z}\phi\right)-i\operatorname{sech}\left(\sqrt{Z}\phi\right)\right)}{\sigma}\right)\varpi\, c_1\\
&-\frac{Z\left(i\sinh\left(\sqrt{Z}\phi\right)+1\right)c_1}{\cosh\left(\sqrt{Z}\phi\right)\left(i\sqrt{Z}-\sqrt{Z}\sinh\left(\sqrt{Z}\phi\right)-\rho\cosh\left(\sqrt{Z}\phi\right)\right)}-\frac{1}{2}\rho\, c_1+\frac{1}{6}\Psi\Bigg),
\end{aligned}
\tag{49}
$$

and

$$
\begin{aligned}
v_{3,8}(t,x) =& -\left(-\frac{1}{2}\frac{\rho}{\sigma}-\frac{1}{4}\frac{\sqrt{Z}\left(\tanh\left(\frac{1}{4}\sqrt{Z}\phi\right)-\coth\left(\frac{1}{4}\sqrt{Z}\phi\right)\right)}{\sigma}\right)\varpi\, c_1\\
&-\frac{1}{4}\frac{Z\left(2\left(\cosh\left(\frac{1}{4}\sqrt{Z}\phi\right)\right)^2-1\right)c_1}{\sinh\left(\frac{1}{4}\sqrt{Z}\phi\right)\cosh\left(\frac{1}{4}\sqrt{Z}\phi\right)\left(-2\rho\sinh\left(\frac{1}{4}\sqrt{Z}\phi\right)\cosh\left(\frac{1}{4}\sqrt{Z}\phi\right)+\sqrt{Z}\right)}-\frac{1}{2}\rho\, c_1+\frac{1}{6}\Psi,\\
w_{3,8}(t,x) =& -s\Bigg(-\left(-\frac{1}{2}\frac{\rho}{\sigma}-\frac{1}{4}\frac{\sqrt{Z}\left(\tanh\left(\frac{1}{4}\sqrt{Z}\phi\right)-\coth\left(\frac{1}{4}\sqrt{Z}\phi\right)\right)}{\sigma}\right)\varpi\, c_1\\
&-\frac{1}{4}\frac{Z\left(2\left(\cosh\left(\frac{1}{4}\sqrt{Z}\phi\right)\right)^2-1\right)c_1}{\sinh\left(\frac{1}{4}\sqrt{Z}\phi\right)\cosh\left(\frac{1}{4}\sqrt{Z}\phi\right)\left(-2\rho\sinh\left(\frac{1}{4}\sqrt{Z}\phi\right)\cosh\left(\frac{1}{4}\sqrt{Z}\phi\right)+\sqrt{Z}\right)}-\frac{1}{2}\rho\, c_1+\frac{1}{6}\Psi\Bigg).
\end{aligned}
\tag{50}
$$

Solution Set. 3.3: When $Z = 0$,

$$
\begin{aligned}
v_{3,9}(t,x) =& 2\frac{\varpi^2\left(\phi\rho+2\right)c_1}{\rho^2\phi}-2\frac{c_1}{\phi\left(\phi\rho+2\right)}-\frac{1}{2}\rho\, c_1+\frac{1}{3}\sqrt{3\,s^2+3},\\
w_{3,9}(t,x) =& -s\left(2\frac{\varpi^2\left(\phi\rho+2\right)c_1}{\rho^2\phi}-2\frac{c_1}{\phi\left(\phi\rho+2\right)}-\frac{1}{2}\rho\, c_1+\frac{1}{3}\sqrt{3\,s^2+3}\right).
\end{aligned}
\tag{51}
$$

Solution Set. 3.4: When $Z = 0$ such that $\rho = 0$ and $\sigma = 0$,

$$\begin{aligned} v_{3,10}(t,x) &= -\frac{1}{6}\,\frac{6\,\varpi^2\phi^2 c_1 - \sqrt{12\,s^2+12}\phi - 6\,c_1}{\phi}, \\ w_{3,10}(t,x) &= -s\Big(-\frac{1}{6}\,\frac{6\,\varpi^2\phi^2 c_1 - \sqrt{12\,s^2+12}\phi - 6\,c_1}{\phi}\Big). \end{aligned} \tag{52}$$

Solution Set. 3.5: When $Z = 0$ such that $\rho = 0$ and $\varpi = 0$,

$$\begin{aligned} v_{3,11}(t,x) &= \frac{1}{6}\,\frac{\sqrt{12\,s^2+12}\phi - 6\,c_1}{\phi}, \\ w_{3,11}(t,x) &= -s\Big(\frac{1}{6}\,\frac{\sqrt{12\,s^2+12}\phi - 6\,c_1}{\phi}\Big). \end{aligned} \tag{53}$$

Solution Set. 3.6: When $\rho = \chi$, $\varpi = \varsigma\chi(\varsigma \neq 0)$, and $\sigma = 0$,

$$\begin{aligned} v_{3,12}(t,x) &= -\left(\mathrm{e}^{\chi\,\phi} - \varsigma\right)\varsigma\chi\,c_1 + \frac{\chi\,\mathrm{e}^{\chi\,\phi}c_1}{\mathrm{e}^{\chi\,\phi} - \varsigma} - \frac{1}{2}\chi\,c_1 + \frac{1}{6}\,\sqrt{-3\chi^2{c_1}^2 + 12\,s^2 + 12}, \\ w_{3,12}(t,x) &= -s\Big(-\left(\mathrm{e}^{\chi\,\phi} - \varsigma\right)\varsigma\chi\,c_1 + \frac{\chi\,\mathrm{e}^{\chi\,\phi}c_1}{\mathrm{e}^{\chi\,\phi} - \varsigma} - \frac{1}{2}\chi\,c_1 + \frac{1}{6}\,\sqrt{-3\chi^2{c_1}^2 + 12\,s^2 + 12}\Big). \end{aligned} \tag{54}$$

Solution Set. 3.7: When $\rho = \chi$, $\sigma = \varsigma\chi(\varsigma \neq 0)$, and $\varpi = 0$,

$$\begin{aligned} v_{3,13}(t,x) &= -\frac{\chi\,c_1}{-1 + \varsigma\,\mathrm{e}^{\chi\,\phi}} - \frac{1}{2}\chi\,c_1 + \frac{1}{6}\,\sqrt{-3\chi^2{c_1}^2 + 12\,s^2 + 12}, \\ w_{3,13}(t,x) &= -s\Big(-\frac{\chi\,c_1}{-1 + \varsigma\,\mathrm{e}^{\chi\,\phi}} - \frac{1}{2}\chi\,c_1 + \frac{1}{6}\,\sqrt{-3\chi^2{c_1}^2 + 12\,s^2 + 12}\Big). \end{aligned} \tag{55}$$

Solution Set. 3.8: When $\rho \neq 0$, $\sigma \neq 0$, and $\varpi = 0$,

$$\begin{aligned} v_{3,14}(t,x) &= \frac{\rho\,(\sinh(\rho\,\phi) - \cosh(\rho\,\phi))\,c_1}{\sinh(\rho\,\phi) - \cosh(\rho\,\phi) - \epsilon_2} - \frac{1}{2}\rho\,c_1 + \frac{1}{6}\,\sqrt{-3\rho^2{c_1}^2 + 12\,s^2 + 12}, \\ w_{3,14}(t,x) &= -s\Big(\frac{\rho\,(\sinh(\rho\,\phi) - \cosh(\rho\,\phi))\,c_1}{\sinh(\rho\,\phi) - \cosh(\rho\,\phi) - \epsilon_2} - \frac{1}{2}\rho\,c_1 + \frac{1}{6}\,\sqrt{-3\rho^2{c_1}^2 + 12\,s^2 + 12}\Big), \end{aligned} \tag{56}$$

and

$$\begin{aligned} v_{3,15}(t,x) &= \frac{\rho\,c_1\epsilon_2}{\cosh(\rho\,\phi) + \sinh(\rho\,\phi) + \epsilon_2} - \frac{1}{2}\rho\,c_1 + \frac{1}{6}\,\sqrt{-3\rho^2{c_1}^2 + 12\,s^2 + 12}, \\ w_{3,15}(t,x) &= -s\Big(\frac{\rho\,c_1\epsilon_2}{\cosh(\rho\,\phi) + \sinh(\rho\,\phi) + \epsilon_2} - \frac{1}{2}\rho\,c_1 + \frac{1}{6}\,\sqrt{-3\rho^2{c_1}^2 + 12\,s^2 + 12}\Big). \end{aligned} \tag{57}$$

Where $\phi = \frac{\Psi c_1}{2s\mu}(x - st)$ in the above solutions of Case 3.

4. Discussion and graphs

In this section, we demonstrate the dynamical behavior of the developed solitary wave solutions. We extract and show several wave patterns using the RMESEM that include kink, anti-kink, cuspon

kink, and bell-shaped bright and dark solutions. A number of 2D graphical representations have been employed to enhance understanding of these solutions that are shown along with carefully chosen parameter values and constraint conditions. These findings under given parameter values are shown in Figures 1–8. The capacity of solitary wave solutions to clarify the fundamental dynamics of intricate physical systems makes them significant.

A kink solitary wave is a particular type of solitary wave that connects two distinct constant asymptotic states as the spatial variable tends to positive or negative infinity. It has a step-like or sigmoid profile, often representing a smooth transition or flip between two stable states. Kink waves commonly occur in systems modeling phase transitions or certain field theories. In the Van der Waals gas model, it happens as a result of transitions in phase, in which the system alternates among states that correspond to shock-like changes in density and pressure. Kink solitary waves are associated with liquid-gas changes in phase in Van der Waals materials and physically characterize slow shifts between two distinct levels of equilibrium in the gas. The antithesis of a kink solitary wave, an anti-kink solitary wave signifies a shift in the other direction. A gas-to-liquid transition, which manifests in the reverse direction of kink solitary waves in a replicating system, is an example of an anti-kink solitary wave that arises when the entire system returns to its initial phase. In general, reverse phase shifts, such as condensing waves in the system of gas that can be connected to wave reflections in restricted Van der Waals gas systems, are represented by the anti-kink solitary wave. A cuspon kink is a kink wave that has a cusp(s) in the profile, representing a hyperbolic profile.

In contrast, hump solitary waves are symmetric and bell-shaped or dip-shaped, often resembling a Gaussian or sech-type pulse. We notably obtained two types of hump waves, namely dark and bright hump waves. A confined dip and negative hump wave in a field, when there is a depression in a variable such pressure or density, travels without altering its shape, is called a dark bell-shaped solitary wave. It happens in low density areas when the mass per unit volume of the gas is smaller than that of its surroundings, making the gas deeper due to fewer intermolecular interactions that may be connected to rarefaction waves. In expanding parts of the gas wherein intermolecular interactions are weaker, a dark bell-shaped solitary wave often indicates areas of lower density or pressure traveling through the fluid. A smooth, confined, positive hump wave that emerges above the backdrop and holds its form while propagating is called a bright bell-like solitary wave. Due to a balance between dispersion as well as nonlinearity in the system as well as Van der Waals interactions, which present attracting forces which encourage localized the compression in density or pressure, these kinds of solitary waves are found in high density regions where the gas operates more like a liquid. Regional density rises within gas molecules or compression waves, in circumstances where intermolecular interactions are significant, are represented by the overall bright bell-like hump solitary wave. These can be correlated with pressure peaks that propagate across the gas medium and may be related to shock formations in actual gases.

In conclusion, dark and bright hump solitary waves indicate regional pressure or density shifts that are essential for comprehending shock development and rarefaction of the waves in real gases, while kink and anti-kink solitary waves indicate phase transition fronts, which are significant for researching gas-liquid interaction and critical events in non-ideal gases.

Figure 1 displays the propagating behaviors of the solitary wave solutions $v_{1,3}(x,t)$ and $w_{1,3}(x,t)$ presented in (21), respectively. In this figure, (a) represents a kink, and (b) represents an anti-kink profile. Figure 2 displays the propagating behaviors of the real, imaginary parts and the squared norms

of the solitary wave solutions $v_{1,7}(x,t)$ and $w_{1,7}(x,t)$ presented in (25), respectively. In this figure, (a) represents a kink, (b) represents an anti-kink, (c) represents bell-shaped bright hump, (d) represents bell-shaped dark hump while the squared norms in (e), and (f) represent anti-kink profiles. Figure 3 displays the propagating behaviors of the the solitary wave solutions $v_{1,8}(x,t)$ and $w_{1,8}(x,t)$ presented in (26), respectively. In this figure, (a) and (b) represent cuspon kink profiles. Figure 4 displays the propagating behaviors of the real and imaginary parts of the solitary wave solution $v_{2,6}(x,t)$ presented in (35). In this figure, (a) represents a bell-shaped bright hump, and (b) represents a lump-like bright-dark hump profile. Figure 5 displays the propagating behaviors of the real and imaginary parts of the solitary wave solution $v_{2,7}(x,t)$ presented in (36). In this figure, (a) represents a bell-shaped bright hump, and (b) represents a lump-like bright-dark hump profile. Figure 6 displays the propagating behaviors of the solitary wave solutions $v_{3,4}(x,t)$ and $w_{3,4}(x,t)$ presented in (46), respectively. In this figure, (a) and (b) represent hump-like kink profiles. Figure 7 displays the propagating behaviors of the real, imaginary parts and the squared norms of the solitary wave solutions $v_{3,6}(x,t)$ and $w_{3,6}(x,t)$ presented in (48), respectively. In this figure, (a) represents an anti-kink, (b) represents a kink, (c) represents bell-shaped bright hump, and (d) represents bell-shaped dark hump, while the squared norms in (e) and (f) represent anti-kink profiles. Finally, Figure 8 displays the propagating behaviors of the squared norms of the solitary wave solutions $v_{3,7}(x,t)$ and $w_{3,7}(x,t)$ presented in (49), respectively. In this figure, (a) and (b) represent anti-kink profiles.

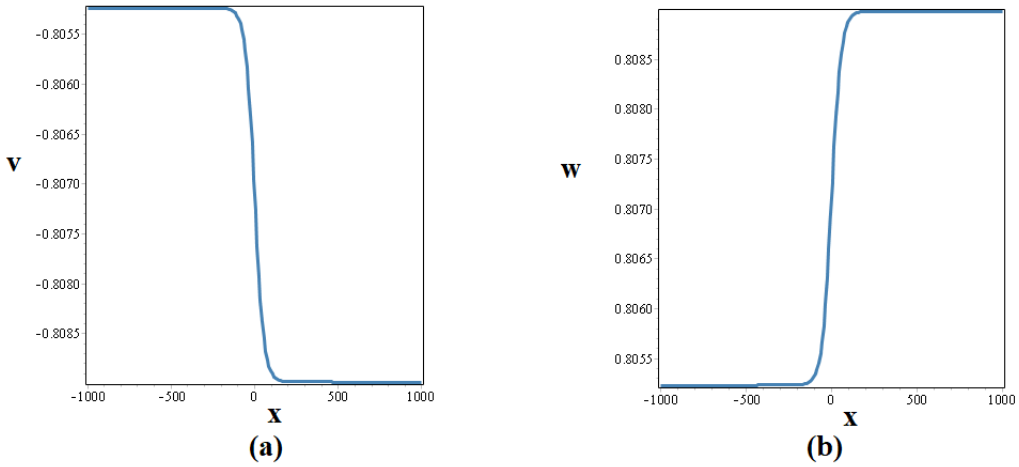

Figure 1. (1 + 1)-dimensional visualization of the solitary wave solutions $v_{1,3}(x,t)$ and $w_{1,3}(x,t)$ presented in (21), respectively, for the parameters' values $\varpi = 1, \rho = 5, \sigma = 4, \mu = 1, s = 1, w_0 = 0.005, t = 0$.

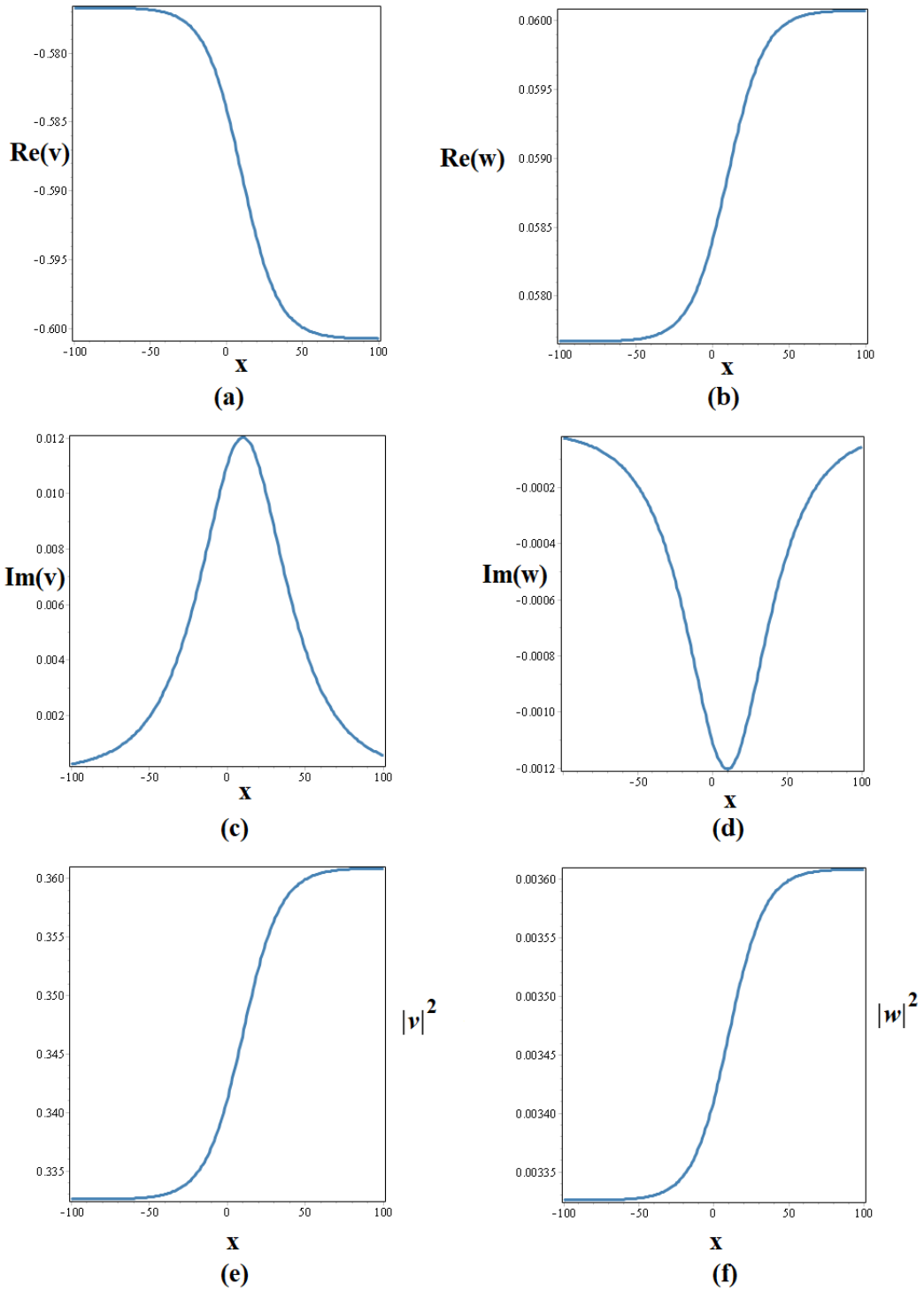

Figure 2. (1 + 1)-dimensional visualization of the real, and imaginary parts and the squared norms of the solitary wave solutions $v_{1,7}(x,t)$ and $w_{1,7}(x,t)$ presented in (25), respectively, for the parameter values $\varpi = 2, \rho = 4, \sigma = 1, \mu = 5, s = 0.10, w_0 = 0.0085, t = 100$.

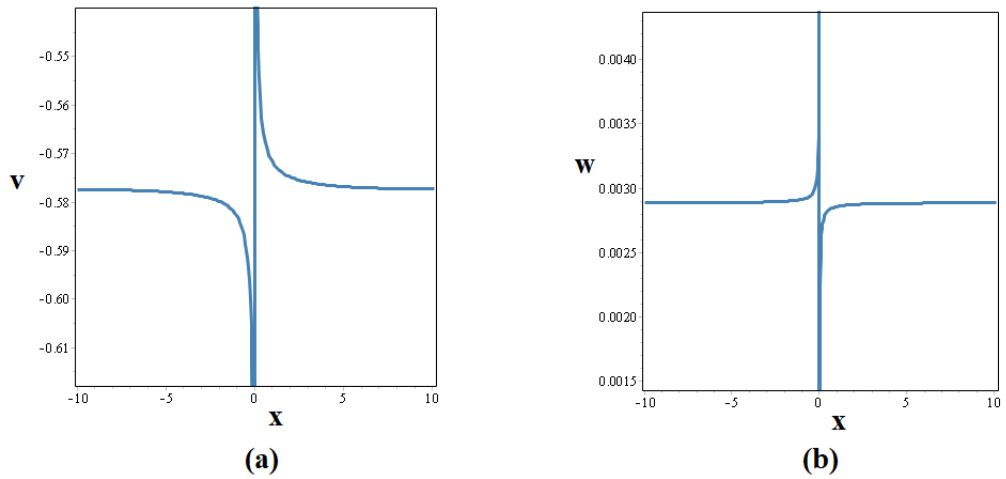

Figure 3. (1 + 1)-dimensional visualization of the the solitary wave solutions $v_{1,8}(x,t)$ and $w_{1,8}(x,t)$ presented in (26), respectively, for the parameter values $\varpi = 3, \rho = 8, \sigma = 3, \mu = 2, s = 0.005, w_0 = 0.003, t = 1$.

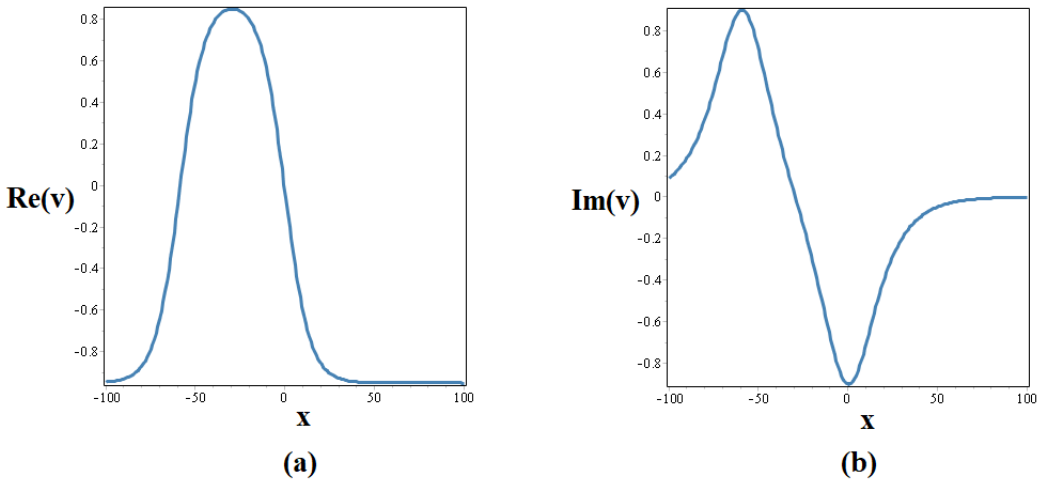

Figure 4. (1 + 1)-dimensional visualization of the real and imaginary parts of the solitary wave solution $v_{2,6}(x,t)$ presented in (35) for the parameter values $\varpi = 3, \rho = 15, \sigma = 1, s = 0, \lambda = 0.005$.

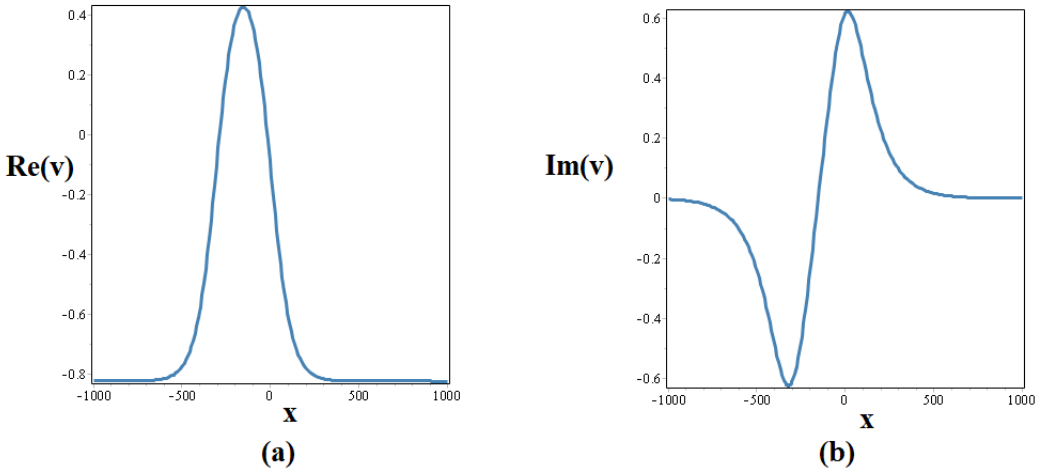

Figure 5. (1 + 1)-dimensional visualization of the real and imaginary parts of the solitary wave solution $v_{2,7}(x,t)$ presented in (36) for the parameter values $\varpi = 2, \rho = 10, \sigma = 3, s = 0, \lambda = 0.001$.

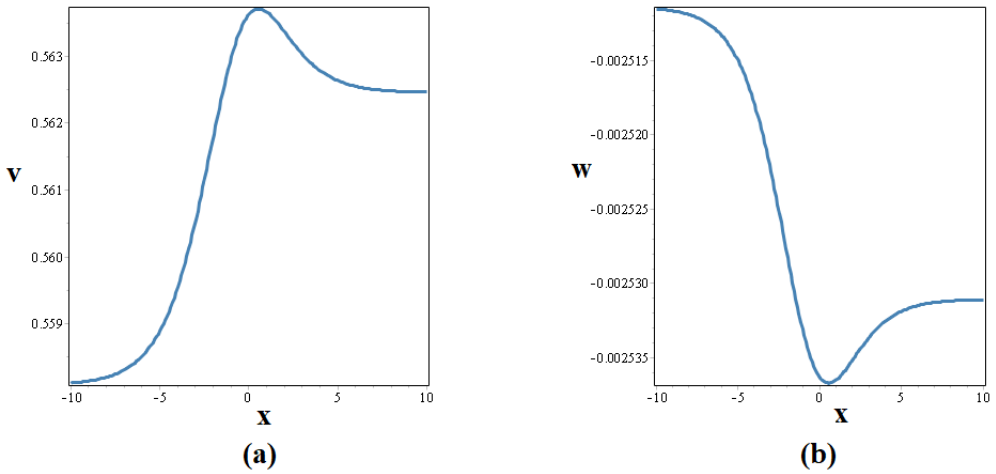

Figure 6. (1 + 1)-dimensional visualization of the solitary wave solutions $v_{3,4}(x,t)$ and $w_{3,4}(x,t)$ presented in (46) respectively for the parameter values $\varpi = 3, \rho = 13, \sigma = 12, \mu = 10, s = 0.0045, c_1 = 0.0035, t = 10$.

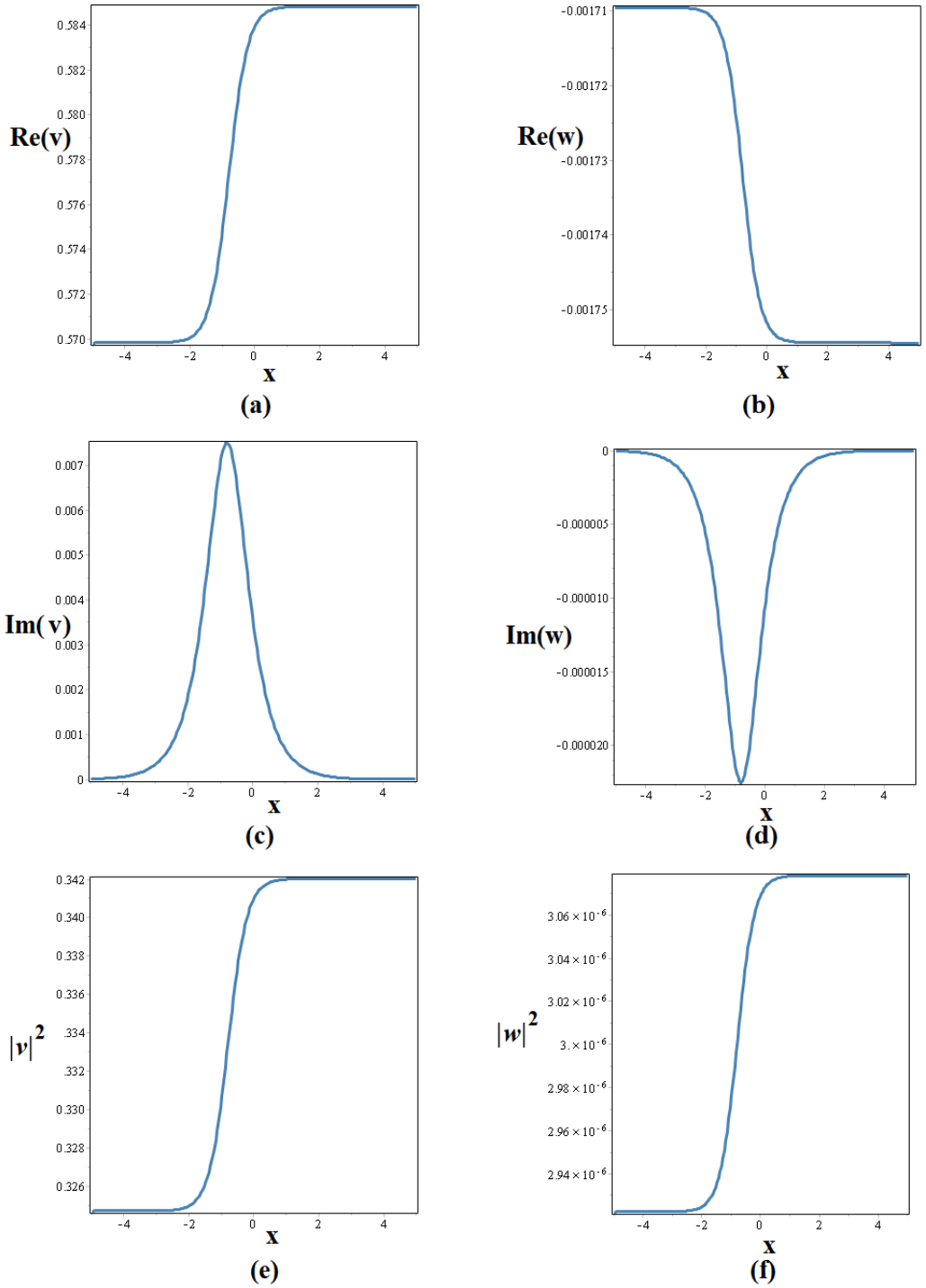

Figure 7. (1 + 1)-dimensional visualization of the real, and imaginary parts and the squared norms of the solitary wave solutions $v_{3,6}(x,t)$ and $w_{3,6}(x,t)$ presented in (48), respectively for the parameter values $\varpi = 4, \rho = 10, \sigma = 4, \mu = 5, s = 0.003, c_1 = 0.0025, t = 0.5$.

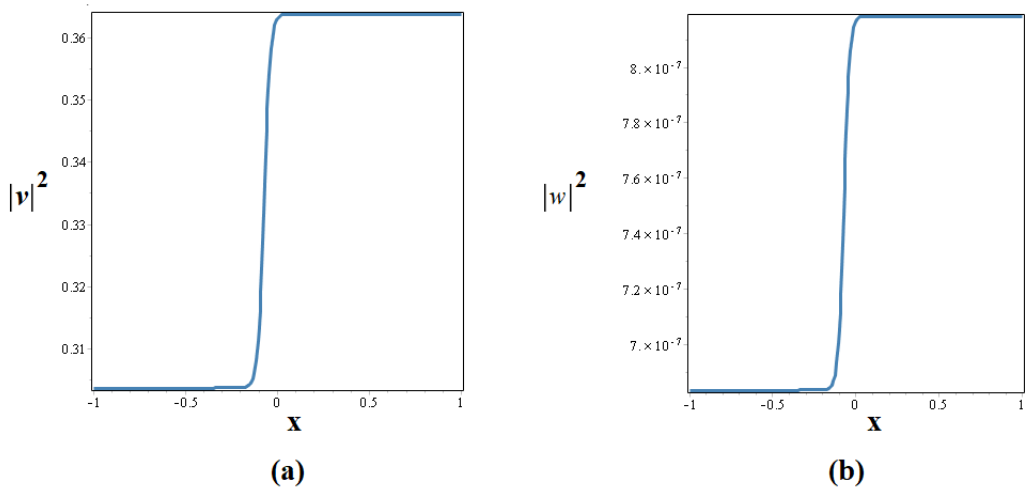

Figure 8. (1 + 1)-dimensional visualization of the squared norms of the solitary wave solutions $v_{3,7}(x,t)$ and $w_{3,7}(x,t)$ presented in (49), respectively for the parameters' values $\varpi = 3, \rho = 10, \sigma = 3, \mu = 2, s = 0.0015, c_1 = 0.0065, t = 0.1$.

5. Conclusions

In summary, this work investigated several features of the (1+1)-dimensional Van der Waals gas system analytically. A novel analytical technique, namely RMESEM, was used to obtain the system's exact solitary wave solutions. By transforming the model into a more manageable NODE, the method was able to derive a range of solitary wave dynamics, including kink, anti-kink, and cuspon kink bright and dark bell-shaped hump wave solutions. Using suitable parameter values that satisfied the constraints, 2D plots were presented to improve comprehension and graphically depict these solutions. Furthermore, we clarify that Case 1's ($c_1 = 0$) and Case 2's ($w_0 = 0$) solutions may correspond to solution structures that can be obtained using other techniques like EDAM, the (G'/G)-expansion method, etc: however, Case 3 produces new wave structures that have not been reported in previous studies. We also observe that maintaining the non-zero integration constant in (14) minimizes solution loss and enables the generation of distinct and varied waveforms, further highlighting the RMESEM's increased adaptability and wider variety of applications. Our proposed RMESEM is a straightforward algebraic ansatz that eliminates the requirement for complex processes like perturbation, linearization, and other transformation procedures that are frequently required in other approaches. Because RMESEM is simple and very effective, we may obtain precise closed-form solutions without the hassles of more complex approaches. The capacity of RMESEM to provide a large number of solution families, such as rational, exponential, hyperbolic, trigonometric, and rational-hyperbolic functions, among others, is one of its main features. By exposing a wide range of wave behaviors that other approaches might miss or be unable to capture, this variety allows for a more thorough examination of the model. Compared to more traditional approaches, RMESEM offers a wide range of solution forms, providing a more thorough and in-depth comprehension of the dynamics present in the model being studied. The efficiency and adaptability of the method in solving a range of nonlinear problems in mathematical science and engineering were validated by the computational analysis. It should be

highlighted, nonetheless, that the suggested approach fails if the largest nonlinear component and the greatest derivative terms do not balance homogeneously. In this case, the technique is unable to balance the nonlinear term with dispersion, which prevents the generation of solitons. Notwithstanding this limitation, the present investigation demonstrates that the methodology employed in this work is highly dependable and successful for nonlinear problems across a range of scientific domains. Finally, future goals of the current research work include a fractional sense analysis and research of the desired model.

Author contributions

Rashid Ali: Conceptualization, methodology, writing-original draft; Rabia Imtiaz: Formal analysis, literature review, writing-review and editing; Moin-ud-Din Junjua: Supervision, project administration, writing-review and editing; Fuad A. Awwad: Data curation, validation, Visualization; Emad A. A. Ismail: Investigation, resources, manuscript revision; Ahmed S. Hendy: Software, visualization, writing-review and editing. All authors have read and approved the final version of the manuscript for publication.

Use of Generative-AI tools declaration

The authors declare that they have not used Artificial Intelligence (AI) tools in the creation of this article.

Funding

This project is supported by King Saud University, Riyadh, Saudi Arabia.

Acknowledgements

Ongoing Research Funding Program, (ORF-2025-1060), King Saud University, Riyadh, Saudi Arabia.

Conflicts of interest

The authors declare no conflict of interest.

References

1. H. K. Ahmed, H. F. Ismael, Optical soliton solutions for the nonlinear Schrödinger equation with higher-order dispersion arise in nonlinear optics, *Phys. Scr.*, **99** (2024), 105276. https://doi.org/10.1088/1402-4896/ad78c3
2. M. A. E. Abdelrahman, H. A. Refaey, M. A. Alharthi, Investigation of new waves in chemical engineering, *Phys. Scr.*, **96** (2021), 075218. https://doi.org/10.1088/1402-4896/abfb24

3. A. Rayal, System of fractal-fractional differential equations and Bernstein wavelets: A comprehensive study of environmental, epidemiological, and financial applications, *Phys. Scr.*, **99** (2025), 025236. https://doi.org/10.1088/1402-4896/ada592
4. P. G. LeFloch, J.-M. Mercier, A class of mesh-free algorithms for some problems arising in finance and machine learning, *J. Sci. Comput.*, **95** (2023), 75. https://doi.org/10.1007/s10915-023-02179-5
5. R. Ali, M. M. Alam, S. Barak, Exploring chaotic behavior of optical solitons in complex structured conformable perturbed Radhakrishnan-Kundu-Lakshmanan model, *Phys. Scr.*, **99** (2024), 095209. https://doi.org/10.1088/1402-4896/ad67b1
6. E. M. E. Zayed, M. E. M. Alngar, A. Biswas, M. Asma, M. Ekici, A. K. Alzahrani, et al., Pure-cubic optical soliton perturbation with full nonlinearity by unified Riccati equation expansion, *Optik*, **223** (2020), 165445. https://doi.org/10.1016/j.ijleo.2020.165445
7. A. Farooq, T. Shafique, M. Abbas, A. Birhanu, Y. S. Hamed, Explicit travelling wave solutions to the time fractional Phi-four equation and their applications in mathematical physics, *Sci. Rep.*, **15** (2025), 1683. https://doi.org/10.1038/s41598-025-86177-7
8. M. Iqbal, W. A. Faridi, R. Ali, A. R. Seadawy, A. A. Rajhi, A. E. Anqi, et al., Dynamical study of optical soliton structure to the nonlinear Landau–Ginzburg–Higgs equation through computational simulation, *Opt. Quant. Electron.*, **56** (2024), 1192. https://doi.org/10.1007/s11082-024-06401-y
9. H. Yasmin, N. H. Aljahdaly, A. M. Saeed, R. Shah, Probing families of optical soliton solutions in fractional perturbed Radhakrishnan-Kundu-Lakshmanan model with improved versions of extended direct algebraic method, *Fractals Fract.*, **7** (2023), 512. https://doi.org/10.3390/fractalfract7070512
10. R. Conte, A. P. Fordy, A. Pickering, A perturbative Painlevé approach to nonlinear differential equations, *Physica D*, **69** (1993), 33–58. https://doi.org/10.1016/0167-2789(93)90179-5
11. Y. L. Xiao, S. Barak, M. Hleili, K. Shah, Exploring the dynamical behaviour of optical solitons in integrable kairat-II and kairat-X equations, *Phys. Scr.*, **99** (2024), 095261. https://doi.org/10.1088/1402-4896/ad6e34
12. H. Khan, Shoaib, D. Baleanu, P. Kumam, J. F. Al-Zaidy, Families of travelling wave solutions for fractional-order extended shallow water wave equations, using an innovative analytical method, *IEEE Access*, **7** (2019), 107523–107532. https://doi.org/10.1109/ACCESS.2019.2933188
13. R. Ali, E. Tag-eldin, A comparative analysis of generalized and extended $\left(\frac{G'}{G}\right)$-Expansion methods for travelling wave solutions of fractional Maccari's system with complex structure, *Alex. Eng. J.*, **79** (2023), 508–530. https://doi.org/10.1016/j.aej.2023.08.007
14. H. Khan, R. Shah, J. F. Gómez-Aguilar, Shoaib, D. Baleanu, P. Kumam, Travelling waves solution for fractional-order biological population model, *Math. Model. Nat. Phenom.*, **16** (2021), 32. https://doi.org/10.1051/mmnp/2021016
15. C. M. Khalique, A. Biswas, A Lie symmetry approach to nonlinear Schrödinger's equation with non-Kerr law nonlinearity, *Commun. Nonlinear Sci.*, **14** (2009), 4033–4040. https://doi.org/10.1016/j.cnsns.2009.02.024

16. N. Li, S. Y. Xu, Y. Z. Sun, Q. Chen, Bright and dark solitons under spatiotemporal modulation in (2+1)-dimensional spin-1 Bose-Einstein condensates, *Nonlinear Dyn.*, **113** (2025), 767–782. https://doi.org/10.1007/s11071-024-10243-4

17. Y. Z. Sun, Z. H. Hu, H. Triki, M. Mirzazadeh, W. J. Liu, A. Biswas, et al., Analytical study of three-soliton interactions with different phases in nonlinear optics, *Nonlinear Dyn.*, **111** (2023), 18391–18400. https://doi.org/10.1007/s11071-023-08786-z

18. Q. Zhou, Y. Z. Sun, H. Triki, Y. Zhong, Z. L. Zeng, M. Mirzazadeh, Study on propagation properties of one-soliton in a multimode fiber with higher-order effects, *Results Phys.*, **41** (2022), 105898. https://doi.org/10.1016/j.rinp.2022.105898

19. L. W. Zeng, J. S. He, B. A. Malomed, J. B. Chen, X. Zhu, Spontaneous symmetry and antisymmetry breaking of two-component solitons in a combination of linear and nonlinear double-well potentials, *Phys. Rev. E*, **110** (2024), 064216. https://doi.org/10.1103/PhysRevE.110.064216

20. L. W. Zeng, M. R. Belić, D. Mihalache, J. C. Shi, J. W. Li, S. Q. Li, et al., Families of gap solitons and their complexes in media with saturable nonlinearity and fractional diffraction, *Nonlinear Dyn.*, **108** (2022), 1671–1680. https://doi.org/10.1007/s11071-022-07291-z

21. J. B. Chen, D. Mihalache, M. R. Belić, J. C. Shi, D. F. Zhu, D. N. Deng, et al., Dark gap solitons in bichromatic optical superlattices under cubic-quintic nonlinearities, *Chaos*, **34** (2024), 113131. https://doi.org/10.1063/5.0232509

22. M. A. S. Murad, H. F. Ismael, T. A. Sulaiman, Various exact solutions to the time-fractional nonlinear Schrödinger equation via the new modified Sardar sub-equation method, *Phys. Scr.*, **99** (2024), 085252. https://doi.org/10.1088/1402-4896/ad62a6

23. Q. Q. Li, J. J. Nie, W. Zhang, Multiple normalized solutions for fractional Schrödinger equations with lack of compactness, *J. Geom. Anal.*, **35** (2025), 59. https://doi.org/10.1007/s12220-024-01897-y

24. Q. Q. Li, J. J. Nie, W. Wang, J. W. Zhou, Normalized solutions for Sobolev critical fractional Schrödinger equation, *Adv. Nonlinear Anal.*, **13** (2024), 20240027. https://doi.org/10.1515/anona-2024-0027

25. D. Gao, X. Lü, M.-S. Peng, Study on the (2+1)-dimensional extension of Hietarinta equation: soliton solutions and Bäcklund transformation, *Phys. Scr.*, **98** (2023), 095225. https://doi.org/10.1088/1402-4896/ace8d0

26. H. Yasmin, A. S. Alshehry, A. H. Ganie, A. M. Mahnashi, R. Shah, Perturbed Gerdjikov-Ivanov equation: Soliton solutions via Backlund transformation, *Optik*, **298** (2024), 171576. https://doi.org/10.1016/j.ijleo.2023.171576

27. M. M. A. Khater, Analytical simulations of the Fokas system, extension (2+1)-dimensional nonlinear Schrödinger equation, *Int. J. Mod. Phys. B*, **35** (2021), 2150286. https://doi.org/10.1142/S0217979221502866

28. J. Manafian, On the complex structures of the Biswas-Milovic equation for power, parabolic and dual parabolic law nonlinearities, *Eur. Phys. J. Plus*, **130** (2015), 255. https://doi.org/10.1140/epjp/i2015-15255-5

29. A. H. Arnous, M. Mirzazadeh, M. S. Hashemi, N. A. Shah, J. D. Chung, Three different integration schemes for finding soliton solutions in the (1+1)-dimensional Van der Waals gas system, *Results Phys.*, **55** (2023), 107178. https://doi.org/10.1016/j.rinp.2023.107178
30. M. Malaver, H. D. Kasmaei, Analytical models for quark stars with van der Waals modified equation of state, *Astrophys. Space Sci.*, **7** (2019), 49–58. https://doi.org/10.11648/j.ijass.20190705.11
31. L. Kipgen, R. Singh, δ-Shocks and vacuum states in the Riemann problem for isothermal van der Waals dusty gas under the flux approximation, *Phys. Fluids*, **35** (2023), 016116. https://doi.org/10.1063/5.0135491
32. E. A. Az-Zo'bi, Solitary and periodic exact solutions of the viscosity-capillarity van der Waals gas equations, *Appl. Appl. Math.*, **14** (2019), 349–358.
33. A. H. Arnous, M. Mirzazadeh, M. S. Hashemi, N. A. Shah, J. D. Chung, Three different integration schemes for finding soliton solutions in the (1+1)-dimensional Van der Waals gas system, *Results Phys.*, **55** (2023), 107178. https://doi.org/10.1016/j.rinp.2023.107178
34. S. Bibi, N. Ahmed, U. Khan, S. T. Mohyud-Din, Some new exact solitary wave solutions of the van der Waals model arising in nature, *Results Phys.*, **9** (2018), 648–655. https://doi.org/10.1016/j.rinp.2018.03.026
35. A. Zafar, B. Khalid, A. Fahand, H. Rezazadeh, A. Bekir, Analytical behaviour of travelling wave solutions to the Van der Waals model, Int. J. Appl. Comput. Math., **6** (2020), 131. https://doi.org/10.1007/s40819-020-00884-5
36. J.-L. Zhang, M.-L. Wang, Y.-M. Wang, Z.-D. Fang, The improved F-expansion method and its applications, *Phys. Lett. A*, **350** (2006), 103–109. https://doi.org/10.1016/j.physleta.2005.10.099
37. E. G. Fan, Extended tanh-function method and its applications to nonlinear equations, *Phys. Lett. A*, **277** (2000), 212–218. https://doi.org/10.1016/S0375-9601(00)00725-8

A. Appendix

The proposed RMESEM, which incorporates Riccati equation, produced a large number of solitary wave solutions in five families, i.e., the exponential, periodic, hyperbolic, rational-hyperbolic, and rational families of solutions. As a result, this incorporation proved beneficial for the selected model. The solutions provided allow us to link the phenomena in the targeted framework to underlying theories and have greatly improved our knowledge of solitary wave dynamics. Limiting our strategy's solutions results in specific solutions for other approaches. An analogy is given in the subsection that follows:

B. Comparison with other analytical methods

The outcomes of our approach are identical to those of several other analytical techniques. For example,

Remarks B.1. The following solution is obtained when $c_1 = 0$ is configured in (15):

$$V(\phi) = \frac{w_0}{\xi(\phi)}. \tag{58}$$

This displays the closed form solution for the F-expansion, EDAM, and tan-function methods. Consequently, our results may also provide the solutions generated by the EDAM, tan-function technique, and F-expansion approach, attaining $c_1 = 0$.

Remarks B.2. Similarly, when $w_0 = 0$ is substituted in Eq (15), the solution structure that follows:

$$V(\phi) = \sum_{l=0}^{1} a_l \left(\frac{\xi'(\phi)}{\xi(\phi)}\right)^l, \tag{59}$$

emerges. This is the series-form solution that emerged by using the (G'/G)-expansion method in conjunction with the Riccati equation.

The results of our study may thus provide a wider range of solutions generated by the (G'/G)-expansion technique [14], the F-expansion method [36], the tan-function method [37], and EDAM [9]. Furthermore, we make it clear that the cases presented in Section 3, that is, Case 1 ($c_1 = 0$) and Case 2 ($w_0 = 0$) correspond to solution structures that can be obtained using other mentioned techniques, but Case 3 results in new wave structures that haven't been documented in earlier research. Furthermore, we point out that maintaining the non-zero integration constant in (14) minimizes solution loss and permits the formation of novel and varied waveforms, highlighting the RMESEM's increased adaptability and wider range of applications.

AIMS Press